Numerical analysis and design of a dynamic system with backlash

Numerical analysis and design of a dynamic system with backlash

E.L.W. Blom 511769
H.M.A. Smetsers 499341
F.J.W. Zeelen 514785
DCT 2005.153

supervisors
dr.ir. R.H.B. Fey
ir. L. Kodde

special thanks to
ir. N.J. Mallon

26th January 2006

Contents

Introduction

In practice many mechanical contain backlash. The desire to eliminate this phenomenon is often hard, if not impossible to realize. Due to the presence of backlash in a system, nonlinear dynamic behavior arises. To get more insight in the behavior of such systems it is useful to analyse these systems experimentally and numerically. Therefore the goal of this investigation is to build an experimental setup that contains backlash and because of that exhibits interesting nonlinear dynamic phenomena. For this purpose, first a numerical analysis will be performed on a theoretical system to get more understanding of the behavior. With the gained experience an actual system will be developed, that resembles the theoretical model as best as possible. When finished, experiments can be done to compare the actual system with the theoretical model. The actual system is also developed to be used as a demonstration model at lectures or presentations.

Chapter 1

Numerical analysis

In this chapter the numerical analysis done, is explained. To get a good feeling for the nonlinear dynamics that occur in a system with backlash first a simple one degree of freedom (1-DOF) system with backlash is analyzed. With this analysis a foundation is made to extend the analysis to the desired experimental setting, a two degrees of freedom system with backlash on both masses and nonlinear behavior within a desired frequency range.

1.1 Requirements for the actual system

The investigation will commence with a numerical analysis of a system with backlash. But because in the end the goal is to achieve an actual prototype, some things have to be kept in mind during this analysis. The theoretical model is depicted in figure 1.1.

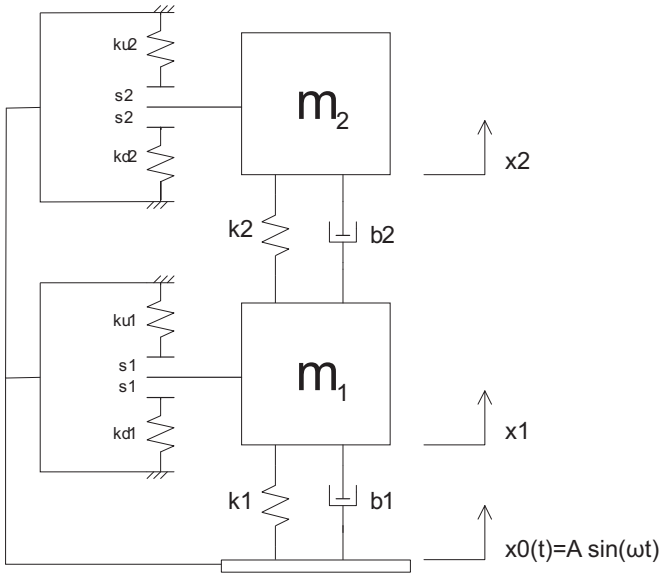

Figure 1.1: The theoretical model

In the figure it can be seen that the ground will have a prescribed motion $s(t)$. This motion will have the form of a sine with amplitude A, that in reality will be realized by a shaker. The shaker available for this purpose has an amplitude of 0.002 m and can handle frequencies between 5 and 60 Hz. These parameters will therefore also be used during the numerical analysis.

Besides this it can be seen in figure 1.1 that the theoretical system contains dampers. In reality no such dampers will be used, probably all the damping in the system will come from material damping. For this damping a value of 3% modal damping is used during the numerical analysis. The backlash is introduced by the springs kd_1, ku_1, kd_2 and ku_2. These springs will come into effect when the backlash s_1 or s_2 is bridged. Because in reality it is easier to attach these springs to the construction itself instead of to the fixed world, this will also be the case during the simulations. This means that the one-sided springs will have the same prescribed motion as the ground. The values of the spring constants will be addressed to later on in this report.

The fact that the actual prototype is also developed for use as a demonstration model imposes another restriction on the system. It should be easy to handle and transport by hand or a small carriage, so the weight and dimensions have to be suitable for this purpose.

1.2 The single degree of freedom system

The simplified system exists of only one mass instead of two. This simplified system is depicted in figure 1.2.

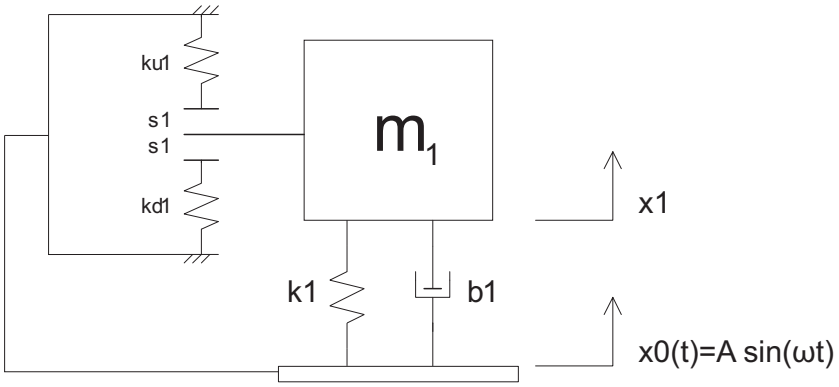

Figure 1.2: The 1DOF system

The parameters for this system will be tuned in such a way that the nonlinear dynamical behavior of the system is clearly visible within the desired frequency range.

On this system, a numerical analysis is performed to visualize the dynamic behavior of the simplified system. The analysis done on the simplified system will develop a feeling for the nonlinear dynamical behavior of a system with backlash. This system will also be used to develop and tune the numerical algorithms that later on will be used to analyze the full experimental system.

1.2.1 Parameter quantification

Because the numerical simulations are meant to be combined with an experimental part, the dimensions of the system have to be adapted to values that can be used in the experimental set-up.

First the frequency range is constrained by the shaker used. This comes down to a frequency range of 5 to 60 Hz. The parameters of the system have to be adapted in such a way that several interesting nonlinear phenomena occur within this frequency range. For the 1DOF linear system the eigenfrequency (ω_n) and the dimensionless damping coefficient (ξ) can be calculated using the following formulas:

$$\omega_n = \sqrt{\frac{k_1}{m_1}}[rad/s] \tag{1.1}$$

$$\xi = \frac{b_1}{2\sqrt{k_1 m_1}} \tag{1.2}$$

To capture the nonlinear behavior (e.g. subharmonic resonances) within the frequency domain, the eigenfrequency is chosen to occur at 15 Hz. With this choice, subharmonic resonances etc will probably occur at about 30 and 45 Hz, which is within the frequency domain. With the assumption that in the experimental setup only material damping will exist, the choice is made to perform simulations with $\xi = 3\%$. With the prototype in mind and the assumption that the masses will be made of steel or aluminium, a reasonable value for m_1 is chosen to be 1 kg. Now we have values for ω_n, ξ and m_1, we can calculate the spring stiffness k_1 and the damping constant b_1.

$$k_1 = \omega_n^2 m_1 = 8882[N/m] \tag{1.3}$$

$$b_1 = 2\xi\sqrt{k_1 m_1} = 5.65[Ns/m] \tag{1.4}$$

For k_{u1} and k_{d1} a value must be chosen large enough, such that interesting non linear behavior arises. But a too high value for these constants will result in numerical problems. Practice has proven that a value of 6 times the value of the linear spring k_1 gives good results [2], so this is maintained throughout the simulations. The amount of backlash s_1 will have different values throughout the analysis.

1.2.2 Equation of motion

The equation of motion of the 1-DOF system can be derived using the Lagrange's equations shown below:

$$\frac{d}{dt}\left[\frac{\partial T}{\partial \dot{q}}\right] - \frac{\partial T}{\partial q} + \frac{\partial V}{\partial q} + Q_{nc} = 0 \tag{1.5}$$

Here:

q denotes the degrees of freedom.
T is the kinetic energy of the system.
V is the potential energy of the system.
Q_{nc} are the non-conservative forces acting on the system.

For the 1-DOF system, as shown in fig 1.2, the movement of the base (x_0) is prescribed by a shaker. For simulation purpose the oscillation of the base plate is modelled as a pure sine with amplitude A [m] and frequency f [Hz]. This gives the following relations for the base plate:

$$\begin{aligned} x_0 &= A\sin(2\pi f t) \\ \dot{x}_0 &= 2A\pi f\cos(2\pi f t) \\ \ddot{x}_0 &= -4A\pi^2 f^2\sin(2\pi f t) \end{aligned} \tag{1.6}$$

Because the movement of the base plate is predetermined, $q = [x_1]$ is the only free coordinate of the system. First the kinematic energy (T) in the system is determined:

$$T = \frac{1}{2} m_1 \dot{x}_1^2 \tag{1.7}$$

This gives:

$$\frac{\partial T}{\partial q} = 0 \tag{1.8}$$

$$\frac{d}{dt}\left[\frac{\partial T}{\partial \dot{q}}\right] = m_1 \ddot{x}_1 \tag{1.9}$$

Secondly the potential energy in the system is determined:

$$V = \frac{1}{2} k_1 (x_1 - x_0)^2 + \frac{1}{2} k_{e1} (x_1 - x_0 - s_1 \cdot \text{sign}(x_1 - x_0))^2 \tag{1.10}$$

With:

$$k_{e1} = \begin{cases} k_{d1} & \text{if} \quad (x_1 - x_0) \leq -s_1 \\ k_{u1} & \text{if} \quad (x_1 - x_0) \geq s_1 \\ 0 & \text{if} \quad -s_1 \leq (x_1 - x_0) \leq s_1 \end{cases}$$

From this it follows that:

$$\frac{\partial V}{\partial q} = k_1 (x_1 - x_0) + k_{e1} (x_1 - x_0 - s_1 \cdot \text{sign}(x_1 - x_0)) \tag{1.11}$$

And finally the non-conservative forces acting on the system (damper) are determined:

$$Qnc = b_1 (\dot{x}_1 - \dot{x}_0) \tag{1.12}$$

With equations 1.8, 1.9, 1.11 and 1.12 the equation of motion for m_1 can be derived:

$$\ddot{x}_1 = -\frac{k_1}{m_1}(x_1 - x_0) - \frac{k_e}{m_1}(x_1 - x_0 - s_1 \cdot \text{sign}(x_1 - x_0)) - \frac{b}{m_1}(\dot{x}_1 - \dot{x}_0) \tag{1.13}$$

1.2.3 Numerical analysis in MatLab

The goal of the analysis is to simulate the behavior of the system in the frequency range of 5 to 60 Hz. For this purpose amplitude frequency diagrams are made of the maximum amplitude of the mass. The standard ODE (Ordinary Differential Equation) solvers present in MatLab, use variable step sizes. To simplify the data processing, explained further on in the section data processing, it is desired to use a fixed step size ODE solver, so for this purpose an algorithm is developed.

The algorithm

The algorithm used is based on a fourth order Runge-Kutta method for numerical integration, just as in the standard ODE-solvers present in MatLab. This method is chosen because it has proven to be fast and accurate, apart from this it is easy to implement. The fourth order Runge-Kutta (rk4) algorithm scheme is:

$$
\begin{aligned}
k_1 &= hf(x_n, t_n) \\
k_2 &= hf(x_n + 1/2h, t_n + 1/2k_1) \\
k_3 &= hf(x_n + 1/2h, t_n + 1/2k_2) \\
k_4 &= hf(x_n + h, t_n + k_3) \\
x_{n+1} &= y_n + 1/6k_1 + 1/3k_2 + 1/6k_4 + O(h^5)
\end{aligned} \tag{1.14}
$$

Here $f(x,t)$ is the non linear differential equation, which can be found in appendix A. The MatLab file that implements the Runge-Kutta method can also be found here. In this method h is the fixed step size. The value for h is determined by trial and error. The performance of the algorithm is compared to a standard algorithm in MatLab and it was concluded that a value of $h = 0.001$ gave good results with respect to accuracy and speed.

Data processing

The data obtained from the ODE solver explained above, is processed to visualize the response of the system (e.g. the amplitude frequency diagrams, phase diagrams, Poincaré points, frequency content of the response and response data). The system will be analyzed using a sweep-up or sweep-down. This means that the system is excited in a frequency and the steady state behavior is awaited before shifting to a higher or lower frequency with a fixed step size.

The amplitude frequency diagrams are extracted from the data using the MatLab file 'frp.m'. In this file the sweep-up (down) data from the simulation is used to calculate the maximum value of the steady-state relative amplitude (e.g. $\max(x_1 - x_0)$) at each excitation frequency.

For the phase diagrams and Poincaré points the MatLab file 'phase.m' is used. This file plots the phase portrait and Poincaré points (of mass 1) in one figure. The number of excitation periods and Poincaré points (n_{tot}) that are used in this plot are adjustable. The Poincaré points are derived by calculating the last sampling point of each oscillation period. The sampling points used are:

$$point = n \times round(\frac{1}{fh})$$

With:
$n \in \mathbb{N}$ and $1 < n \leq n_{tot}$
f, the excitation frequency
h, fixed step size used in simulation
$round()$, MatLab function that rounds any real number to it's nearest integer number

The response and frequency content are calculated with the MatLab file 'dft.m', in which the number of excitation periods plotted is adjustable. Furthermore the frequency content is derived using 'discrete fourier transformation' of the response data ('dft_calc.m'). The standard frequency resolution used in this file is 0.25 Hz.

All the data processing files can be found in appendix C. For further information on the use of data processing files also see appendix D.

1.2.4 Numerical analysis in AUTO

Next to the selfmade algorithm in MatLab, another method is used to perform simulations. The program is called AUTO and uses Fortran code. The advantage with AUTO is that it solves two-point boundary value problems to calculate periodic solutions and therefore can also find unstable periodic solutions. In MatLab, initial value problems are solved and only stable periodic solutions can be found.

1.2.5 Verification

Verification of the shaker

First the prescribed excitation of the shaker $x_0(t)$ will be verified by plotting it's movement. The excitation is simulated for a time period of 2 seconds. The first second, the parameters are set to a frequency of 3 Hz and an amplitude of 0.002 m and the following second the frequency is set to 6 Hz while keeping the amplitude constant. This is similar to what will be done during the simulations on the model. The result of the test is shown in figure 1.3.

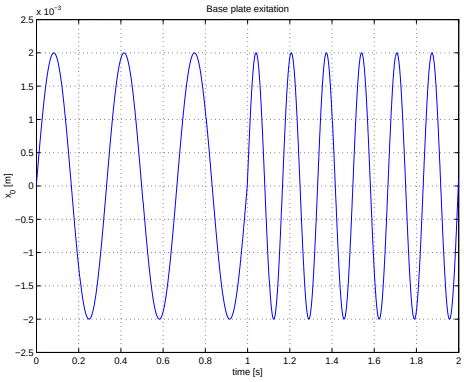

Figure 1.3: The excitation of the floor $s(t)$ versus time

The figure clearly shows that the shaker is modelled in the correct way.

Algorithm verification

Subsequently, to check whether the algorithm works, it will be compared with the standard ODE-solver 'ode45.m' in MatLab. The response of the 1DOF model, for $q_0 = [0, 0]$ and $f = 15Hz$, is determined with both algorithms and the results are shown in figure 1.4 and figure 1.5.

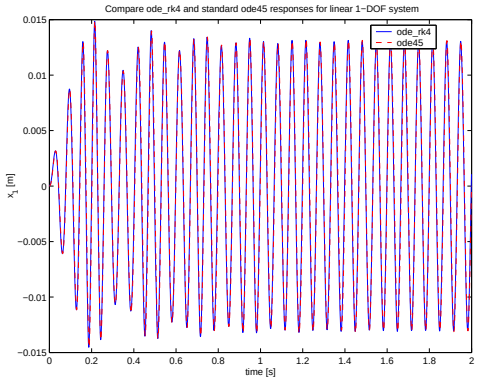

Figure 1.4: Comparison of responses calculated with ode45.m and ode_rk4.m

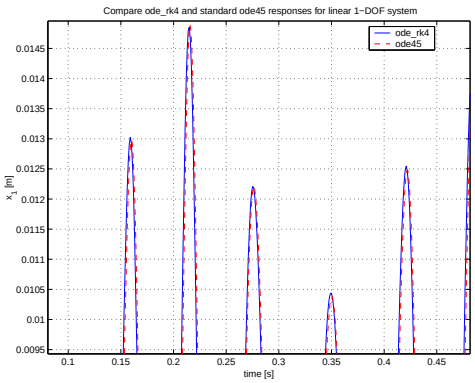

Figure 1.5: Comparison of responses in peaks

The figures show that both algorithms result in the same solution so one may assume that ode_rk4.m works.

Model verification

Finally, to check whether the system is modelled in the right way, first a simulation will be done of the linear system without backlash. With the settings chosen, the peak of the eigenfrequency should lie at 15 Hz. The result of the simulation is depicted in figure 1.6.

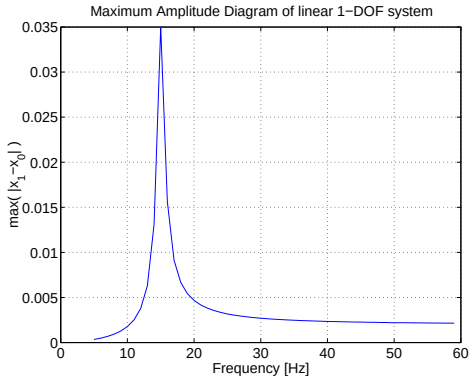

Figure 1.6: The amplitude frequency diagram of the linear 1DOF system

It can be seen that the results show the expected peak at 15 Hz, which strengthens the confidence in the model. The last test on the model and the numerical tools used (MatLab, AUTO), consists of a comparison between AUTO and MatLab results. The tests are done on the 1-DOF model with both non linear springs and a backlash of 10 mm. In figure 1.7 a MatLab simulation of the 1-DOF model is performed both for increasing frequency (sweep up) and for decreasing frequency (sweep down).

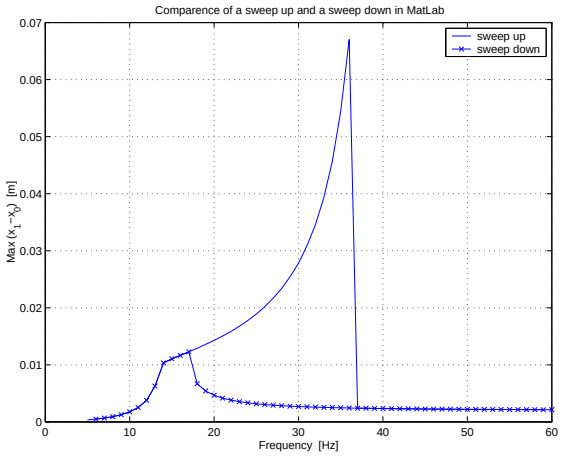

Figure 1.7: Amplitude frequency diagrams of 1-DOF model in MatLab with non linear springs on both down and upper side resulting from a sweep up and a sweep down

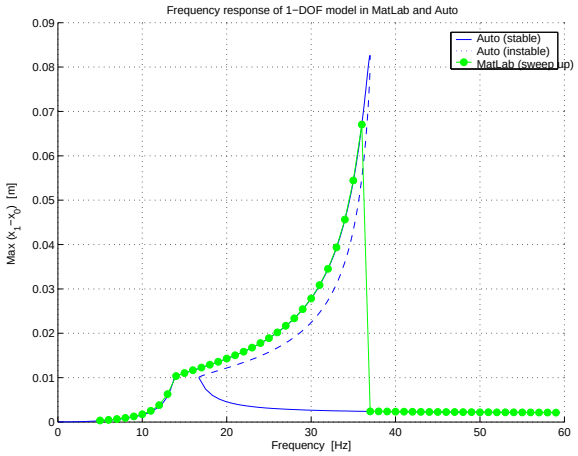

Figure 1.8: Amplitude frequency diagrams of 1-DOF model with non linear springs on both down and upper side resulting from a sweep up in MatLab and from AUTO

The simulations show different solutions for sweep up and down because between about 15 to 35 Hz there are multiple solutions of the differential equation. MatLab can only find one (stable)

solution at a time and at the cyclic fold bifurcation point it will jump to a solution on another branch. In this case for the sweep up this happens on another point compared to the sweep down. The advantage of using AUTO is that it can find also find unstable solutions that cannot be found by MatLab. The result of the simulation in AUTO is plotted in figure 1.8 together with the 'sweep up' in MatLab. Apart from the fact that now the solutions of the sweep up and sweep down of figure 1.7 are better comprehended, one can also see that both methods give the same solution. This confirms the correctness of the model.

1.2.6 Simulation results

Analysis with one nonlinear spring on the downside (s=0 mm)

With the model and the ODE solvers checked the simulations can start. To get a good feeling of what backlash does to the dynamical behavior of the system, first only one nonlinear spring will be added to the linear system. First the backlash will be set at 0 $[m]$ to realize nonlinear behavior. As described in [2] it is likely that a $1/n$th subharmonic resonance peak will arise at about nf_{nonlin} [Hz], with $n = 2, 3, 4, \ldots$. The harmonic resonance peak at f_{nonlin} [Hz] will, in comparison to the linear system, probably shift to a higher frequency because of the stiffness of the nonlinear spring. An estimation for this frequency is given in [1] by:

$$f_{nonlin} = \frac{2\sqrt{1+\alpha}}{1+\sqrt{1+\alpha}} f_{lin} \tag{1.15}$$

Here:
f_{nonlin} is the harmonic resonance frequency of the nonlinear system.
f_{lin} is the resonance frequency of the linear system
α is the ratio between the nonlinear spring and the linear spring ($\frac{k_c}{k}$)

With the settings, $\alpha = 6$ and $f_{lin} = 15$Hz, this gives a nonlinear resonance frequency of $f_{nonlin} = 21.7$Hz.

MatLab and the m-files in appendix C are used to calculate the amplitude frequency plot of this system. This is done by calculating the steady-state behavior of the system at frequencies ranging from 5 to 60 Hz (sweep-up) with steps of 1 Hz. The result of this is shown below.

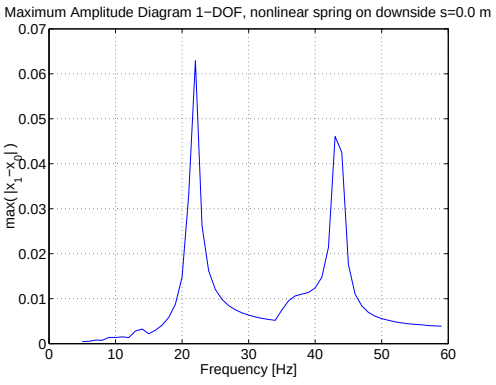

Figure 1.9: The amplitude frequency diagram of the 1DOF system

The amplitude frequency diagram in figure 1.9 shows that the predictions made above are correct. The first resonance peak has shifted to a higher frequency, 22 Hz instead of 15 Hz as found for the linear system. A 1/2 subharmonic resonance peak arises at about 44 Hz.

The response of the system in the first resonance peak (at 22 Hz) is shown in figures 1.10 and 1.11. It shows that the response of the system with a base frequency of 22 Hz is a harmonic solution.

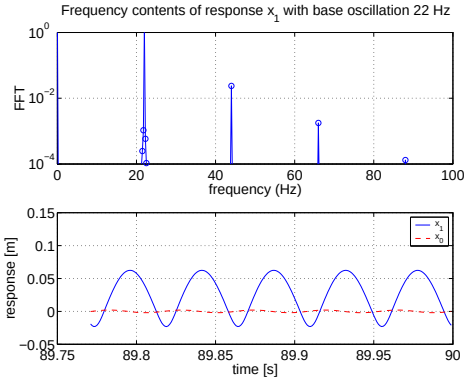

Figure 1.10: 1DOF system response with base excitation 22 Hz

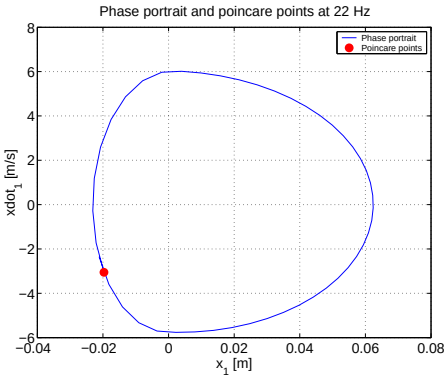

Figure 1.11: 1DOF system phase portrait with base excitation 22 Hz

From the phase portrait and response of the system at the second resonance peak at 44 Hz, as shown in fig 1.12 and 1.13, can be concluded that this is a 1/2 subharmonic solution. This is also visible in the phase portrait with two Poincaré points. A 1/2 subharmonic solution means that the base frequency of the response (x_1) is $\frac{1}{2}$ times the excitation frequency. The frequency content of the response shows that the excitation frequency is also present in the response but that the contribution of the half subharmonic frequency to the response is much larger. The power term at 0 Hz is non-zero because the mean of the response is not equal to zero. An interesting observation is that the response of the system at 22 Hz is almost equal to the response of the system at 44 Hz.

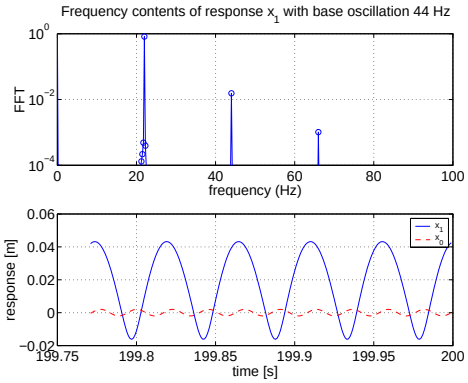

Figure 1.12: 1DOF system response with base excitation 44 Hz

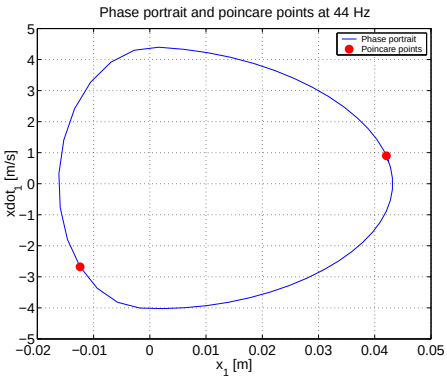

Figure 1.13: 1DOF system phase portrait with base excitation 44 Hz

The amplitude frequency diagram of figure 1.9 also shows a small resonance peak around 14 Hz. The response of the system at this frequency is shown in figures 1.14 and 1.15. The Poincaré points in the phase portrait show that this also is a half subharmonic resonance (two points). The frequency content shows that at this excitation frequency (14 Hz), the response of the system also contains higher frequencies of n times the base frequency of 7 Hz.

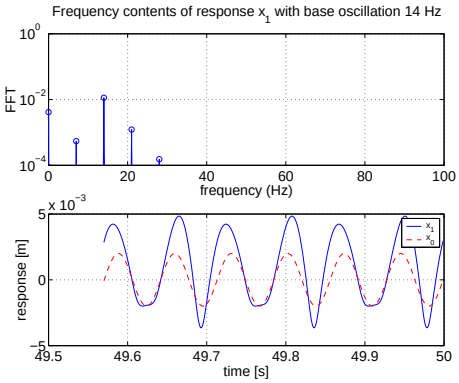

Figure 1.14: 1DOF system response with ground excitation 14 Hz

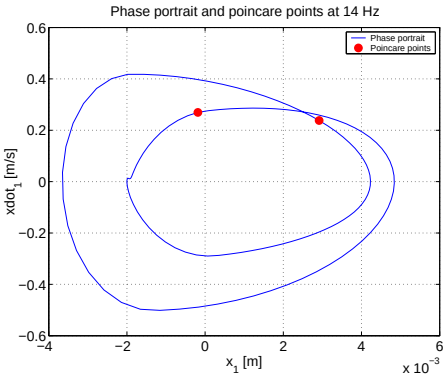

Figure 1.15: 1DOF system phase portrait with ground excitation 14 Hz

All the responses shown above show that adding a nonlinear spring to the linear system has a huge effect on the response of the system. All simulation results that are shown above are without backlash ($s = 0$ mm). The next step in evaluating the system is to add backlash to the system.

Analysis with one non linear spring on the downside (s=10 mm)

For the next simulations a backlash of 10 mm is introduced to the system. This value is derived from the fact that at this length the backlash is bridged when the excitation frequency is near the first eigenfrequency. The system with backlash will behave like a linear system when $x_1 - x_0 < s$ during the whole periodic solution. Because the start of the subharmonic resonance peak is below 10 mm there will probably be no subharmonic resonance peak when sweep-up or sweep-down is used to construct the amplitude frequency diagram.

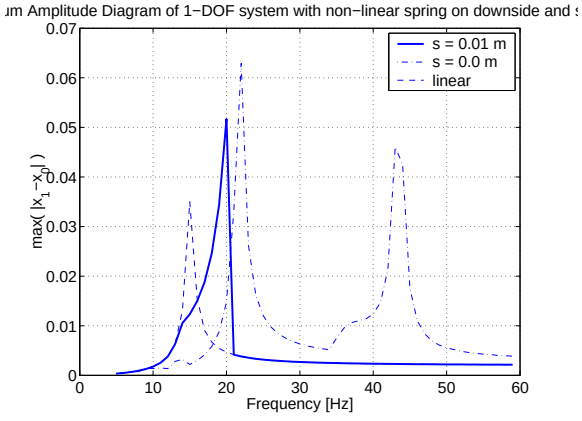

Figure 1.16: The amplitude frequency diagram of the 1-DOF system with a backlash of 1 cm

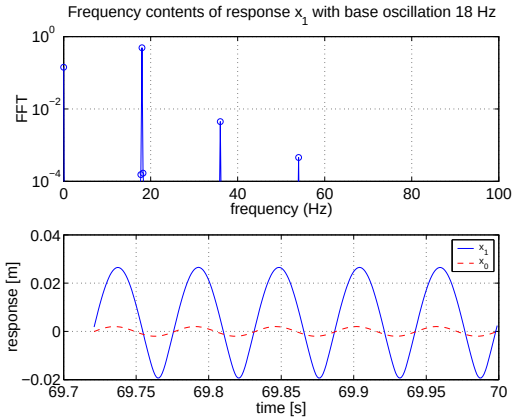

Figure 1.17: 1DOF system response portrait with ground excitation 18 Hz

The amplitude frequency diagram shows that below $max(x_1 - x_0) = 10$ mm the response is identical to the linear system. When the backlash ($max(x_1 - x_0) > 10$ mm) is bridged by the moving mass, the nonlinear spring contributes to the response. In the response diagram this is shown as a kink in the response curve (at 14 Hz). The amplitude frequency diagrams of the previous simulations (linear and $s = 0$ mm) are also plotted in the graph to see the relation of this response to the previous ones.

When the nonlinear spring is reached by the mass, the response of the system becomes nonlinear, as shown in figure 1.17. The resonance peak of the system with backlash is an intermediate form of the two other plots. When the backlash becomes smaller, the resonance peak will slowly converge to the one where $s = 0$ mm. On the other hand, the peak will converge to the linear resonance peak when the backlash becomes larger. When the backlash is larger than the highest amplitude of the linear resonance peak, the system will not be able to touch the nonlinear spring and the response will be the same as the linear system.

In the amplitude frequency plot of figure 1.16 a sudden jump in amplitude occurs at the right hand side of the resonance peak. The amplitude of the response suddenly drops from the top of the peak to the linear response line. Because the MatLab algorithm used only finds stable solutions the program AUTO is used to check the reason for this. The result of the AUTO simulation is compared to the MatLab result in figure 1.18.

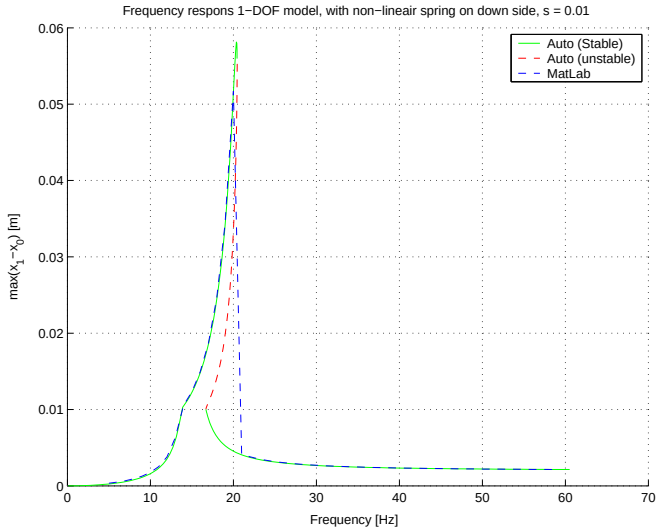

Figure 1.18: Comparison of AUTO and MatLab results

The AUTO results show that there is an unstable branch of harmonic solutions between the nonlinear resonance peak and the linear solution branch. This implies that the solution found with MatLab is correct. It is hard to find the other stable solution (from 16 to 21 Hz) with MatLab, this is probably because the domain of attraction of this solution is very narrow and small transient behavior (when switching to a higher or lower frequency) will 'push' the system to the stable high amplitude solution. This probably happens when the nonlinear spring is 'touched' by the mass due to transient behavior (when switching the excitation frequency).

The amplitude frequency plot also shows that the subharmonic resonance peak disappears. This is the case because for $s = 10$ mm the backlash is not bridged by the system at the point where the peak starts (+/- 34 Hz). When the backlash is smaller than the relative amplitude of the system at this frequency, the subharmonic peak will appear as shown in figure 1.19. Here a gap of 2 mm is used. The figure also shows that the subharmonic resonance peak is suddenly aborted in the same way as the first resonance peak in figure 1.17.

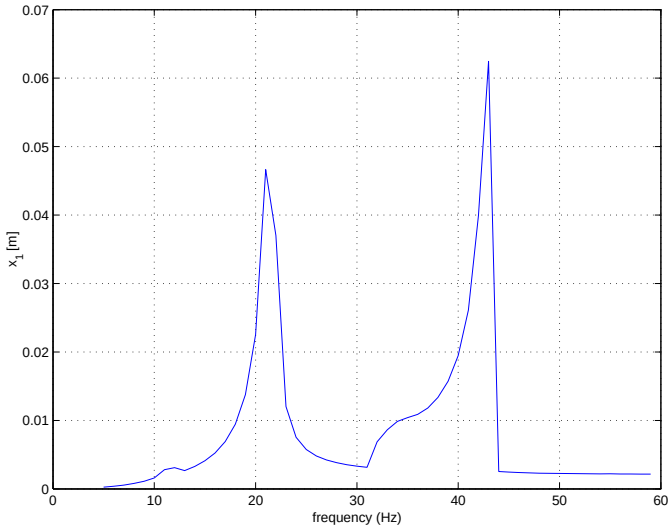

Figure 1.19: 1-DOF amplitude frequency diagram with a backlash of 2 mm

Analysis with two non linear springs

The final simulation of the one degree of freedom system is done with two nonlinear springs, k_{u1} and k_{d1} in figure 1.2. The α factor for both springs is chosen to be 6. Simulations are done both in MatLab and AUTO, the results of this were also used in section 1.2.5, figures 1.7 and 1.8. For a clear representation only AUTO results are used here, see figure 1.20. In figure 1.20 the result of a simulation with two nonlinear springs and $s = 10$ mm is shown. The AUTO result shows a large resonance peak leaning to the right. The base of this resonance peak is the same as the base of the linear 1-dof system (also shown in the plot). When the relative amplitude of the system becomes larger than the backlash (10 mm), the linear path is abandoned and the peak starts to lean to the right.

In the figure also the response of the system with two nonlinear springs and $s = 0$ mm is shown. For this situation the frequency of the resonance peak is easily calculated with:

$$\frac{1}{2\pi}\sqrt{\frac{k_1 + k_e}{m_1}} = \frac{1}{2\pi}\sqrt{\frac{k_1 + \alpha k_1}{m_1}} = \sqrt{1+\alpha} \times f_{lin} \tag{1.16}$$

An estimation for the frequency that the leaning peak tends to, is $\sqrt{1+\alpha} \times f_{lin}$. This implies that when the backlash is reasonably small in comparison to the height of the linear resonance peak, the frequency range over which the nonlinear peak leans can be estimated. For this system this range is:

$$f_{lin} = 15\text{Hz to } \sqrt{1+\alpha} \times f_{lin} = \sqrt{7} \times 15 = 39.7\text{Hz} \tag{1.17}$$

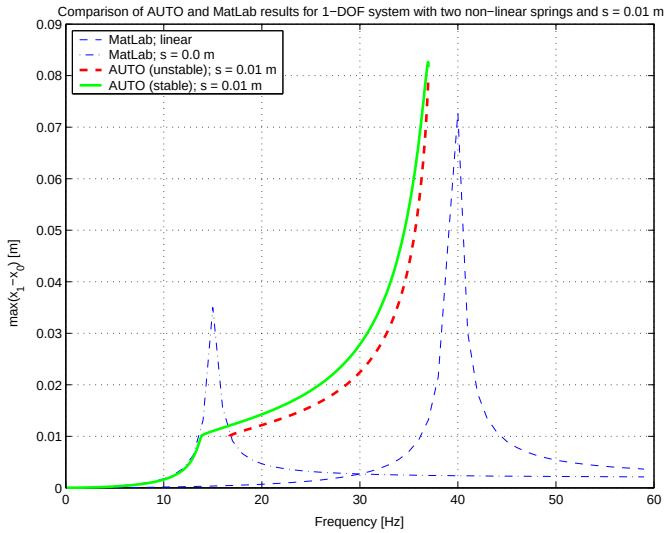

Figure 1.20: Amplitude frequency diagram with two nonlinear springs

1.3 The two degree of freedom system

Now some knowledge of nonlinear dynamic behavior has been obtained, an analysis of the originally intended two degrees of freedom system of figure 1.21 can be made.

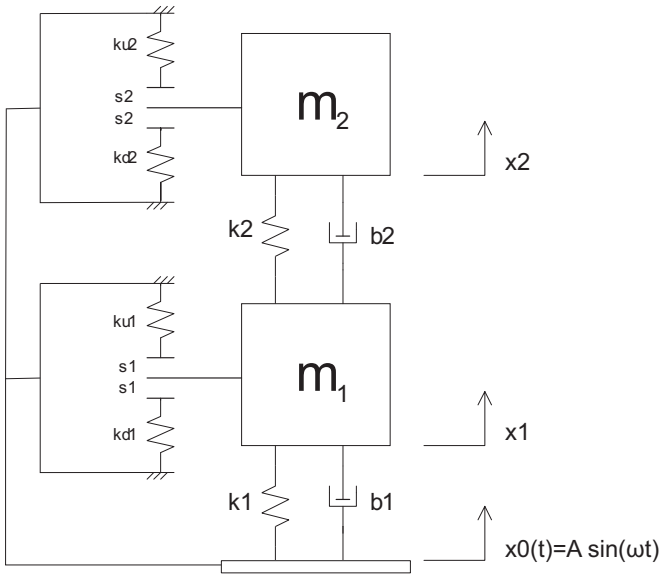

Figure 1.21: The 2-DOF model

1.3.1 Parameter quantification

Just as for the 1-DOF system, the parameters of the 2-DOF model are tuned in such a way that interesting nonlinear behavior will occur within the frequency range of 5 to 60 Hz.

The eigenfrequencies of the linear 2-DOF system can be calculated from the characteristic equation:

$$(k_1 + k_2 - \omega_i^2 m_1)(k_2 - \omega_i^2 m_2) - k_2^2 = 0 \tag{1.18}$$

With the assumption that both m_1 and m_2 are 1 kg, this gives:

$$\omega_i^2 = \frac{(k_1 + 2k_2) \pm \sqrt{(k_1 + 2k_2)^2 - 4k_1k_2}}{2} \qquad i = 1, 2 \tag{1.19}$$

In figure 1.22 these eigenfrequencies are plotted for different combinations of k_1 and k_2 in a contour-plot. The point indicated by the arrow is a combination of k_1 and k_2 for which the eigenfrequencies occur around 10 and 25 Hz. This is the chosen combination because these eigenfrequencies both fit well into the frequency range.

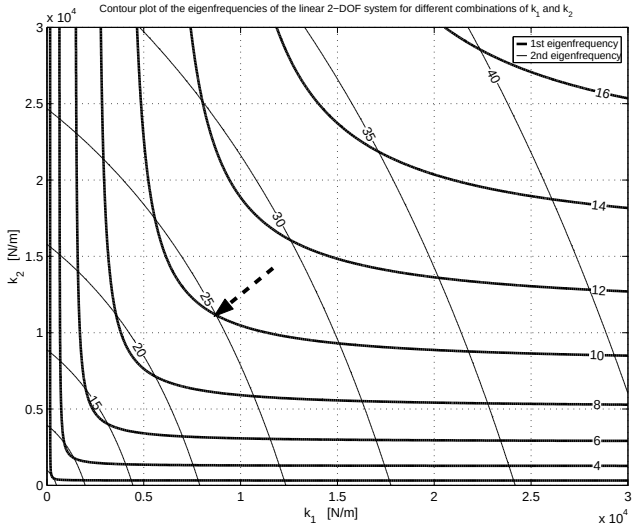

Figure 1.22: The eigenfrequencies of the linear 2-DOF model for different combinations of k_1 and k_2

The corresponding values for k_1 and k_2 are 8735 and 11150 [N/m]. And for these values following from Eq. 1.19, the eigenfrequencies occur at 9.5 Hz and 26.4 Hz.

Now the mass matrix and stiffness matrix of the linear system are known, the damping matrix is determined. This will be done using Rayleigh damping, which means that the damping matrix is proportional to the mass and stiffness matrices:

$$\mathbf{C} = \eta\mathbf{M} + \delta\mathbf{K} \tag{1.20}$$

Using this damping matrix the modal equations will be uncoupled:

$$2\omega_n\xi_n = \phi_n\mathbf{C}\phi_n \tag{1.21}$$

This equation can be rewritten as:

$$2\omega_n\xi_n = \eta + \delta\omega_n^2 \tag{1.22}$$

With ω_1=20π, ω_2=50π and the choice ξ_1=0.03 and ξ_2=0.03 (i.e. the system is slightly damped), this gives:

$$\eta = 2\omega_1\omega_2(\xi_1\omega_2 - \xi_2\omega_1)/(\omega_2^2 - \omega_1^2) = 2.6279 \tag{1.23}$$

$$\delta = 2(\xi_2\omega_2 - \xi_1\omega_1)/(\omega_2^2 - \omega_1^2) = 2.6628 \cdot 10^{-4} \tag{1.24}$$

The values of the nonlinear springs are again chosen to be equal to 6 times the values of the linear springs, so $k_{1d} = k_{1u} = 6k_1$ and $k_{2d} = k_{2u} = 6k_2$.

1.3.2 Equations of motion

The equations of motion of the 2-DOF system can again be derived using Lagrange's equations.

The movement of the base is the same as before (Eq 1.6), so there are no changes in x_0.

Because now there are two masses, q changes into q=$[x_1,x_2]^T$. Again, first the kinetic energy (T) of the system is determined:

$$T = \frac{1}{2}m_1\dot{x}_1^2 + \frac{1}{2}m_2\dot{x}_2^2 \tag{1.25}$$

This gives:

$$\frac{\partial T}{\partial q} = \begin{bmatrix} 0 \\ 0 \end{bmatrix} \tag{1.26}$$

$$\frac{d}{dt}\left[\frac{\partial T}{\partial \dot{q}}\right] = \begin{bmatrix} m_1\ddot{x}_1 \\ m_2\ddot{x}_2 \end{bmatrix} \tag{1.27}$$

Secondly the potential energy in the system is determined:

$$V = \frac{1}{2}k_1(x_1-x_0)^2+\frac{1}{2}k_2(x_2-x_1)^2+\frac{1}{2}k_{e1}(x_1-x_0-s_1\cdot\text{sign}(x_1-x_0))^2+\frac{1}{2}k_{e2}(x_2-x_0-s_2\cdot\text{sign}(x_2-x_0))^2 \tag{1.28}$$

With:

$$k_{e1} = \begin{cases} k_{d1} & \text{if} \quad (x_1 - x_0) \leq -s_1 \\ k_{u1} & \text{if} \quad (x_1 - x_0) \geq s_1 \\ 0 & \text{if} \quad -s_1 \leq (x_1 - x_0) \leq s_1 \end{cases}$$

and

$$k_{e2} = \begin{cases} k_{d2} & \text{if} \quad (x_2 - x_0) \leq -s_2 \\ k_{u2} & \text{if} \quad (x_2 - x_0) \geq s_2 \\ 0 & \text{if} \quad -s_2 \leq (x_2 - x_0) \leq s_2 \end{cases}$$

From this it follows that:

$$\frac{\partial V}{\partial q} = \begin{bmatrix} k_1(x_1 - x_0) + k_2(x_1 - x_2) + k_{e1}(x_1 - x_0 - s_1 \cdot \text{sign}(x_1 - x_0)) \\ k_2(x_2 - x_1) + k_{e2}(x_2 - x_0 - s_2 \cdot \text{sign}(x_2 - x_0)) \end{bmatrix} \tag{1.29}$$

As said in section 1.3.1 the damping will be modelled using Rayleigh damping (Eq 1.20). The non-conservative forces now become:

$$Q_{nc} = \begin{bmatrix} (\eta m_1 + \delta(k_1 + k_2))(\dot{x}_1 - \dot{x}_0) - \delta k_2(\dot{x}_2 - \dot{x}_0) \\ -\delta k_2(\dot{x}_1 - \dot{x}_0) + (\eta m_2 + \delta k_2)(\dot{x}_2 - \dot{x}_0) \end{bmatrix} \tag{1.30}$$

With equations 1.26, 1.27, 1.29 and 1.30 the equations of motion for m_1 and m_2 can be derived:

$$\begin{aligned} \ddot{x}_1 &= -\frac{k_1}{m_1}(x_1 - x_0) + \frac{k_2}{m_1}(x_2 - x_1) - \frac{k_{e1}}{m_1}(x_1 - x_0 - s_1 \cdot \text{sign}(x_1 - x_0)) \\ &\quad -\frac{1}{m_1}((\eta m_1 + \delta(k_1 + k_2))(\dot{x}_1 - \dot{x}_0) - \delta k_2(\dot{x}_2 - \dot{x}_0)) \end{aligned} \tag{1.31}$$

$$\begin{aligned} \ddot{x}_2 &= -\frac{k_2}{m_2}(x_2 - x_1) - \frac{k_{e2}}{m_2}(x_2 - x_0 - s_2 \cdot \text{sign}(x_2 - x_0)) \\ &\quad +\frac{1}{m_2}(\delta k_2(\dot{x}_1 - \dot{x}_0) + (\eta m_2 + \delta k_2)(\dot{x}_2 - \dot{x}_0)) \end{aligned} \tag{1.32}$$

1.3.3 Model Verification

To verify the 2-DOF model, two tests are performed. First the linear system will be simulated and the eigenvalues found are compared to the theoretical eigenvalues. Secondly, simulation results obtained with MatLab will be compared to results obtained with AUTO. The results are shown in respectively figure 1.23 and 1.24.

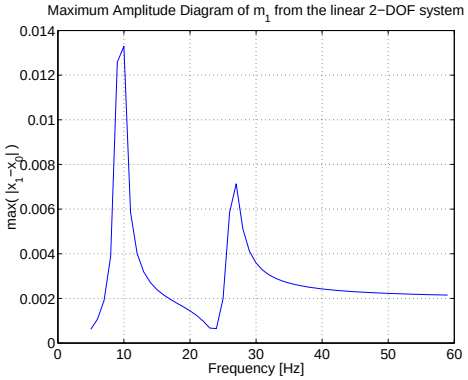

Figure 1.23: Verifying the 2-DOF model by a check of the eigenvalues

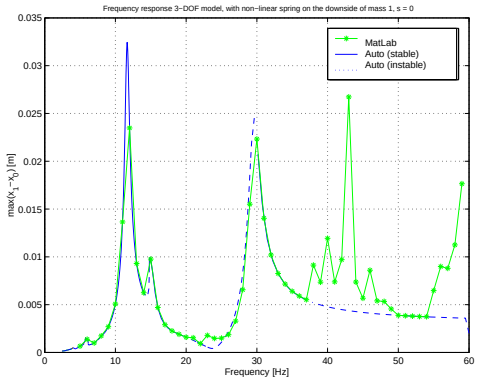

Figure 1.24: Comparison of MatLab and AUTO implemented on the 2-DOF model

Figure 1.23 shows that the resonance frequencies resulting from the simulations in MatLab correspond to the eigenfrequencies of 9.5 and 26.4 Hz. Figure 1.24 shows that the simulations done in MatLab correspond well to the simulations in AUTO. Considering the results of these two tests, one can assume the models are correctly implemented.

1.3.4 Simulation results

In this section the simulations with the 2-DOF system will be explained and evaluated. In the first simulations that will be carried out only the nonlinear spring on the downside of the lower mass (k_{d1} on m_1) is active without backlash ($s_1 = 0$ mm). This simulation will be extended with the introduction of backlash ($s_1 > 0$ mm). After that, simulations will be done with multiple nonlinear springs and backlash in the system. Because the introduction of nonlinear springs has a huge effect on the dynamics of the 2-DOF system, the results shown are just a brief overview of all interesting dynamics this system comprehends.

One nonlinear spring on the downside of mass 1 and $s_1 = 0$ mm

For the first simulation on the 2-DOF system only the nonlinear spring k_{d1} without backlash ($s_1 = 0$ mm) is used. With these settings a MatLab sweep-up simulation is executed. The amplitude frequency plot of this simulation is shown below.

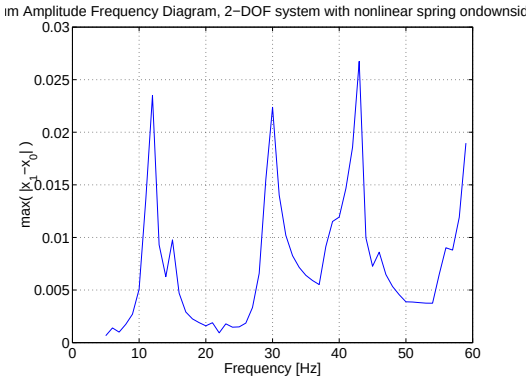

Figure 1.25: The amplitude frequency plot of the 2-DOF model with k_{d1} and $s_1 = 0$ mm

This figure clearly shows that the addition of only one nonlinear spring on mass 1 has a tremendous impact on the dynamical behavior of the system in comparison to the linear response shown in figure 1.23. The resonance peaks from the linear case have shifted to a higher frequency, which was also the case for the 1-DOF system. The second thing that stands out is that some new resonance peaks arise (near 15, 43 and 60 Hz). Also some 'non-smooth' sections occur in the figure (near 22 and 46 Hz).

First the response of the system at the two main resonance peaks are evaluated, as shown in figure 1.26 and 1.27.

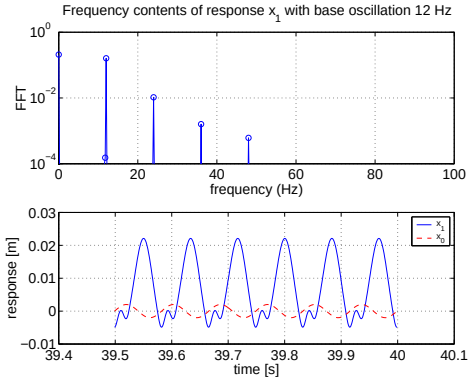

Figure 1.26: Response and frequency content at 12 Hz

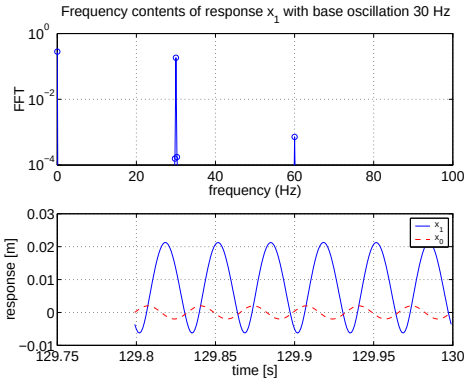

Figure 1.27: Response and frequency content at 30 Hz

The responses show that at these excitation frequencies the system has a harmonic solution, which implies that these are the main resonance peaks (also visible in the linear system).

Two other interesting frequencies seem to be 15 Hz, at which a small peak arises, and 43 Hz, where a huge peak arises. The responses of the system at these frequencies are depicted in figure 1.28 and 1.29.

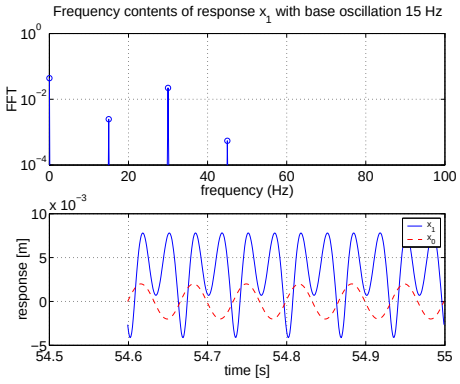

Figure 1.28: Response and frequency content at 15 Hz

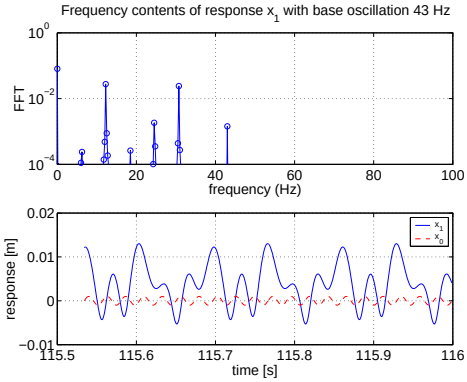

Figure 1.29: Response and frequency content at 43 Hz

The response at 15Hz shows that there is a harmonic solution. This is confirmed by the frequency content where the base frequency is the same as the excitation frequency. The interesting aspect of

the frequency content is that not the excitation frequency, nor the base frequency has the biggest contribution. In this case the biggest contribution to the response is supplied by 2 times the excitation frequency, which implies that here a 2^{nd} superharmonic resonance exists.

The response in the peak at 43 Hz shows that there is a $1/7^{th}$ subharmonic solution. This is confirmed by the frequency content, that shows a base frequency of 6 Hz, which is $6/43 \approx 1/7$ times the excitation frequency.

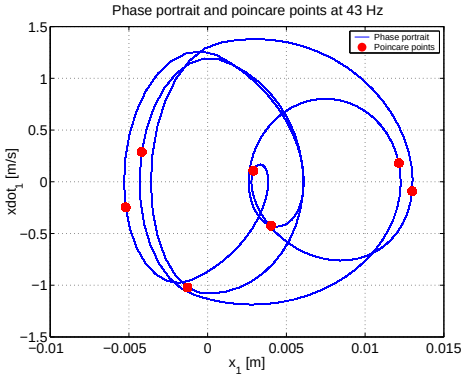

Figure 1.30: Plot of 2000 Poincaré points and the phase portrait for the 2-DOF model with k_{d1} and $s_1 = 0$

Figure 1.30, which is a plot of the Poincaré points for 2000 excitation periods, confirms this too. The figure clearly shows 7 Poincaré points and a clear and smooth phase portrait that is exactly the same for each period. A last remark with respect to the frequency content is that the excitation frequency is approximately the sum of both eigenfrequencies while these frequencies are most dominant in the frequency content.

The last region of the amplitude frequency plot for these settings that will be examined is the region near 21 Hz. Figure 1.31 shows that AUTO gives an unstable solution for this frequency, while MatLab results in a small peak.

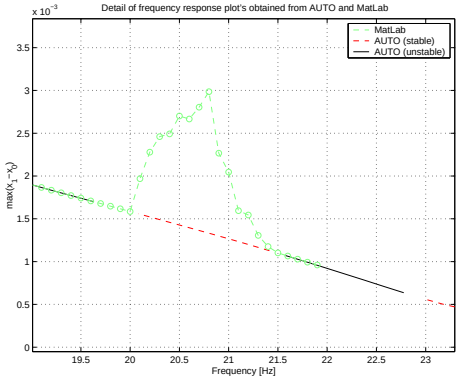

Figure 1.31: The amplitude frequency plot of the 2-DOF model with k_{d1} and $s_1 = 0$ in the region of 21 Hz

In figure 1.32 the response for a frequency of 21 Hz is plotted. Also a plot of the Poincaré points is made for 2000 excitation periods (Fig. 1.33). The figure shows that the solution may be quasi-periodic because the form is a closed curve.

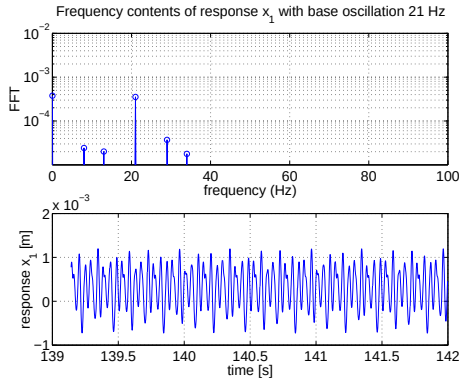

Figure 1.32: Response and frequency content at 21 Hz

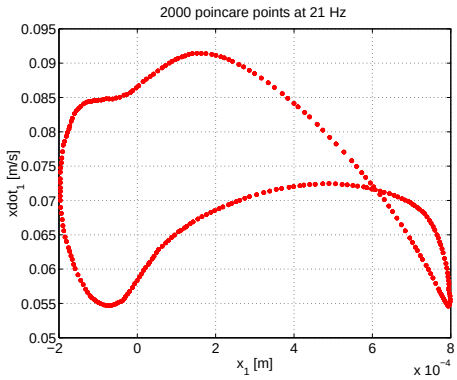

Figure 1.33: Plot of Poincaré points at 21 Hz for 2000 oscillation periods

The corresponding phase portrait is plotted for 50 oscillations periods (Fig. 1.34).

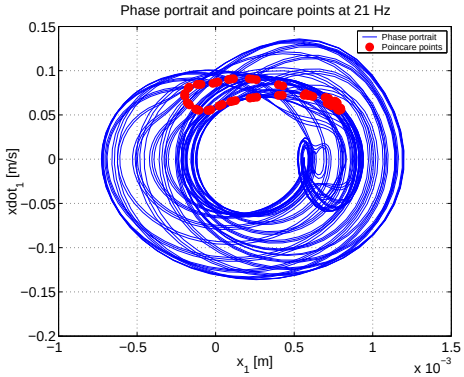

Figure 1.34: Plot of the Poincaré points and the phase portrait for 50 oscillation periods

One nonlinear spring on the downside of mass 1 with $s_1 = 5$ mm

The next step in doing simulations on the 2-DOF model is the introduction of backlash of s_1=0.005 m, while keeping the remaining settings the same. The amplitude frequency plot resulting from these settings is depicted in figure 1.35. Just as for the 1-DOF model, the introduction of backlash eliminates several resonance peaks.

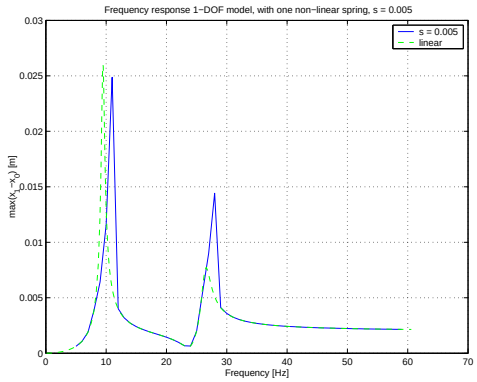

Figure 1.35: Amplitude frequency plot in MatLab Hz

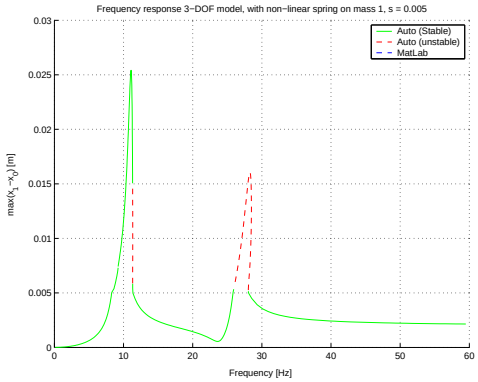

Figure 1.36: Amplitude frequency plot in AUTO

The amplitude frequency diagram is also determined in AUTO, resulting in figure 1.36. From this figure the conclusion can be drawn that the second harmonic resonance peak is unstable and therefore this will be an interesting region for further examination.

The response of the system for a ground excitation of 28 Hz can be found in figure 1.37 and figure 1.38 shows the Poincaré points with the phase portrait.

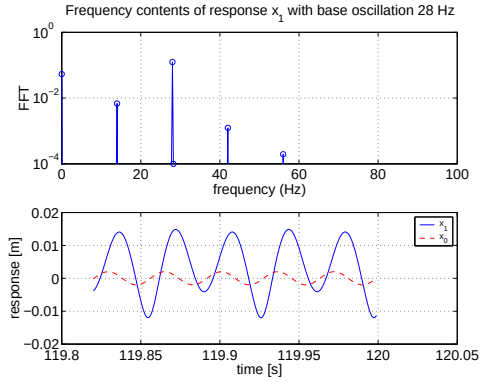

Figure 1.37: The response and frequency content at 28 Hz

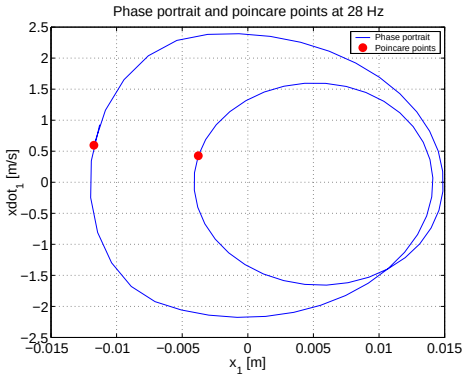

Figure 1.38: Plot of Poincaré points and phase portrait at 28 Hz

The results clearly indicate a 1/2 subharmonic solution.

Using multiple non linear springs

In this last section results will be presented from two other settings with more than one non linear spring to give the reader an idea of what to expect when more springs are added. The results are only presented in figures and will not be explained using the approach of the previous sections. The results are presented only in amplitude frequency plots, calculated using both MatLab (only sweep-up) and AUTO.

Figure 1.39 shows the amplitude frequency plot for the 2-DOF model with two nonlinear springs on m_1 and figure 1.40 the amplitude frequency plot for two nonlinear springs in both m_1 and m_2.

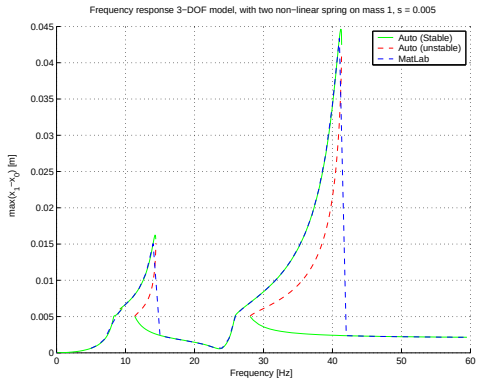

Figure 1.39: The amplitude frequency plot for two non linear springs on m_1

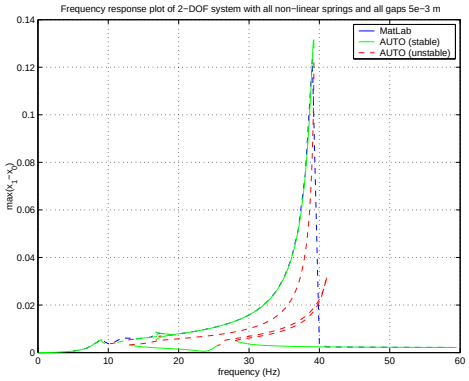

Figure 1.40: The amplitude frequency plot for two non linear springs on both m_1 and m_2

1.4 Conclusion and recommendations

During the simulations a lot of knowledge has been gained on the nonlinear dynamic behavior of the system with various settings. This knowledge has provided insight in some problems that can occur during the simulations, during the data processing and most important in practice. Furthermore some ideas have arisen about issues that may be interesting to investigate in the future.

From the simulations it can be concluded that with the settings used, interesting nonlinear dynamic behavior occurs in the desired frequency range. The key settings and assumptions made are:

Parameter / Setting	**Value**
Eigenfrequencies	$f_{n1} = 10$Hz, $f_{n2} = 25$Hz
Damping	+/- 3% (uncoupled)
Frequency range	5 to 60Hz
Excitation	$x_0 = A\sin(\omega t)$, with $A = 0.002$ m

With these settings, the simulation results are satisfying with respect to the dynamical behavior shown. When looking more closely at the results it shows that with some settings (e.g. two nonlinear springs on both m1 and m2) the maximum amplitude of the 2-DOF system is very large, namely +/- 120 mm. Numerically this value causes no difficulties, nevertheless when we look at the final experimental setup it is not desirable or even possible. Because when designing a prototype which uses a shaker with a fixed displacement of 2 mm, and the system is oscillating with a amplitude of 120 mm it is clear that the dimensioning of the prototype will be a problem. Another problem with this shaker setting is that the acceleration will increase quadratical with the frequency. In the simulations done this results in enormous accelerations, which probably can not be realized in the real experimental setup.

When experimenting on the prototype, designed in the next chapter, it might be useful to excite the ground in another way than used throughout the simulations. When the maximum deviation the prototype can withstand is a lot smaller than the deviations found during simulations, a solution can be to decrease the amplitude of the excitation (A). For low frequencies this will not be a problem in practice, but for higher frequencies this will (due to the quadratic increase) still result in enormous forces acting on the excitation mechanism. A way to solve this problem is to use a fixed velocity or fixed acceleration. In figure 1.41 can be seen what this does to an arbitrary

frequency response plot. The amplitudes used for the velocity and acceleration are those necessary to achieve a displacement amplitude of 0.002 m at a frequency of 5 Hz and these are kept constant throughout the frequency domain.

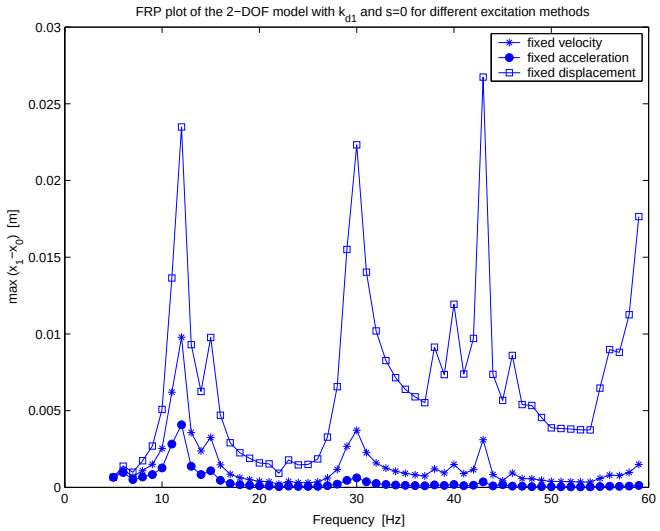

Figure 1.41: FRP plot of the 2-DOF model for different excitation methods

The figure shows that especially for higher frequencies the height of the peaks decreases considerable. This means that the acceleration and therefore the forces decrease a lot as well. For further investigation it is useful to tune the excitation method to the maximal amplitude that the real prototype can withstand / is designed for. When doing this it has to be kept in mind that the amplitude of the interesting resonance peaks have to be sufficiently large enough measuring or for applying backlash.

The settings / limitations that occur in the design of the prototype have to be used as feedback for tuning the simulation parameters. The end result of doing this will be that the simulation model and prototype are alike and the nonlinear dynamics are still 'visible'. Achieving this will be the main target of the future work with respect to the numerical analysis within this project.

Chapter 2

The design of a prototype

2.1 Introduction

The numerical simulations of the previous chapter are all performed to get more understanding of the dynamical behavior of a system with backlash, but they also provide the foundation for the design of a prototype. The simulations have given an idea about what to expect in practice and this knowledge must be kept in mind in the design. The prototype that is designed in this chapter needs to resemble the dynamical behavior of the abstract system shown below as best as possible.

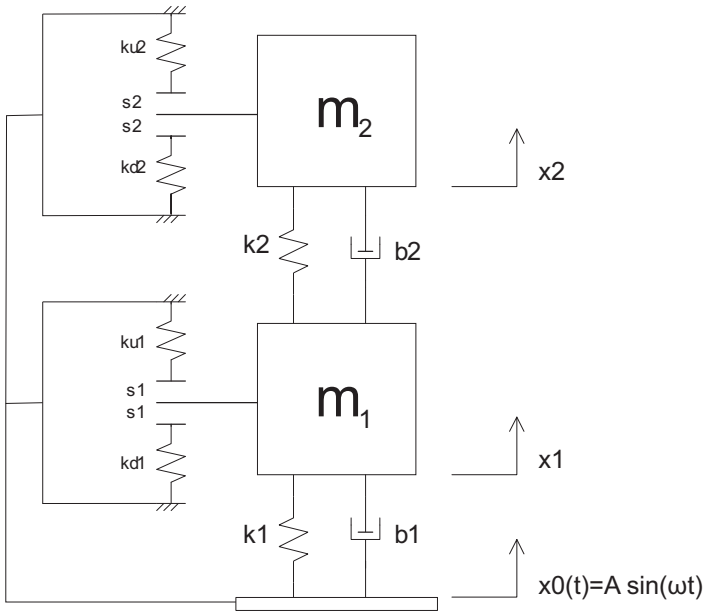

Figure 2.1: 2-DOF system

In this chapter several proposals for a design will be presented and discussed. The designs will be judged on six criteria, namely: one dimensional movement, complexity, implementation of backlash, ability of parameter variation (other mass or spring values), accessibility (for e.g. sensors), the compatibility with simulations and the appearance. Furthermore an investigation will be done after dimensioning of one of the designs and a measuring plan will be constructed. At the end some conclusions will be drawn.

2.2 Design 1: Cylinder piston construction

The first design is the so called 'cylinder piston construction' (CPC design). The base of this construction is a cylindrical holder in which the masses (pistons) can translate. A graphical representation of the design is shown in figure 2.2.

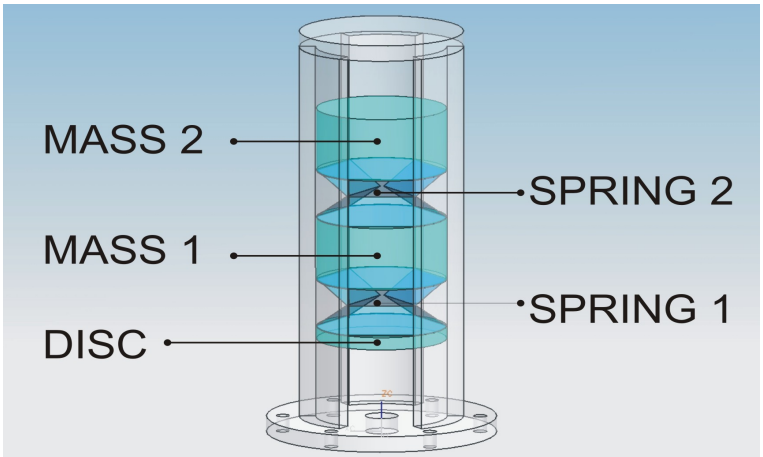

Figure 2.2: Graphical representation of the CPC design

Inside the holder, the masses and linear springs are placed. To prescribe the harmonic motion to the masses and holder, the lower spring and holder can be fixed on the shaker.

The lower linear spring (complete with mounting discs) is mounted on the shaker and attached to the lower mass. The upper linear spring is attached to the lower mass and the upper mass. With this configuration the movement of the shaker is elastically (lower spring) passed on to the lower mass. Subsequently the movement of the first mass is elastically (upper linear spring) passed on to the second mass.

The backlash in the system can be created by making slots in de walls of the holder which contain the nonlinear springs and backlash. Three additional blocks of material on the sides of the masses (at an angle of 120 degrees from each other) reach out through the slots and can touch the nonlinear springs when the backlash is bridged.

The linear springs attached to the masses consist of three folded 'leafsprings' (made out of one sheet of metal), which are mounted on two small discs. The ends of the spring are positioned at the most outer radius of the piston under an angle of 120° according to the centreline of the mass. Due to this positioning the construction will now have a thermal midpoint in the centreline of the total cylinder piston construction. Hereby, thermal changes will not affect the orientation of the bodies with respect to each other, and so measurements will not be affected by a change in the ambient temperature. By the use of three 'leafsprings' at an angle of 120 degrees with respect to each other, the tilt of the pistons in the holder is also reduced to a minimum.

Because of the open spaces in the holder the movement of the masses can be seen from the outside, which is a good feature for demonstration purposes. Another advantage is that the sensors can be mounted easily at the moving parts. The electric cables can directly come out of the construction without making room for cables in the construction.

Desirable is a hysteresis free system (no dissipation of energy). Because of friction between the holder and the masses this will certainly not be the case. Friction can be lowered in several ways (e.g. lubrication, different material), nevertheless this is no option because friction has to be completely eliminated from the system.

Below can be found to what extend the design answers the design criteria:

Design Criterium	Judgement
movement	- (friction)
complexity	+
implementation of backlash	-
parameter variation	+/-
accessibility (for e.g. sensors)	+
compatibility with simulations	++
appearance	++

2.3 Design 2: Hanging masses

The next design is very basic and is called the hanging masses design. A portal is fixed on the shaker and the actual system is hanging on the top center. The system consists from top to bottom of; a leafspring (spring1), a mass (mass1), a leafspring (spring 2) and a mass (mass 2). The portal moves back and forth along with the shaker (figure 2.3), and forces the 2-DOF masses and spring system to move. Due to its design both masses can undergo several rotations. The first is a rotation round the vertical z-axis, which can result in a wobbling movement. The second only affects mass 2 and is a rotation around the y-axis. These two rotations can be eliminated by adding two leafsprings, which can be seen in figure 2.4. The last inconsistency in the movement of the masses is a small lift in the z-direction of the masses. This affects mass 2 more than mass 1, but the absolute severeness of this problem is not investigated. This last rotation is a lot harder to eliminate and will not be examined for this design.

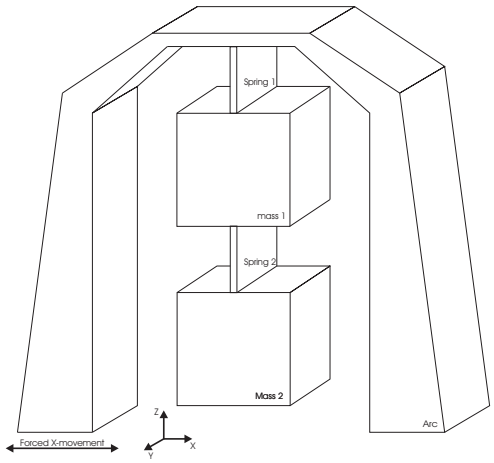

Figure 2.3: The hanging masses design

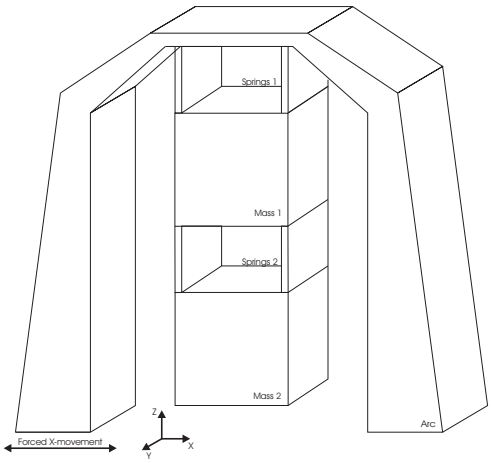

Figure 2.4: The improved hanging masses design

The nonlinear springs can be attached in the sidewalls of the portal after removing parts of the sidewalls (Fig 2.5). On the masses some impact rods have to be made that come in contact with these springs. These additions can be made in the form of thick, short rod with screw thread on it. These rods can then be screwed into the mass and be adjusted to get the desired amount of backlash. The ends of the rods must be rounded to get a good impact (figure 2.6).

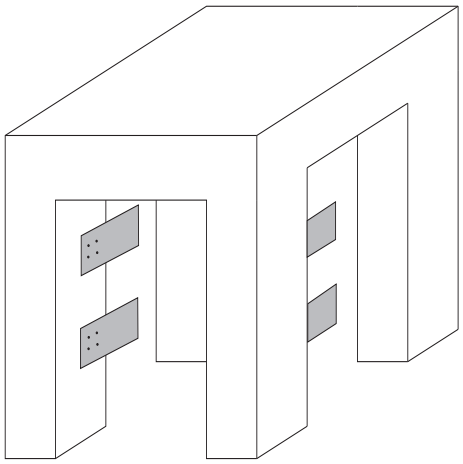

Figure 2.5: The adapted portal including non linear springs

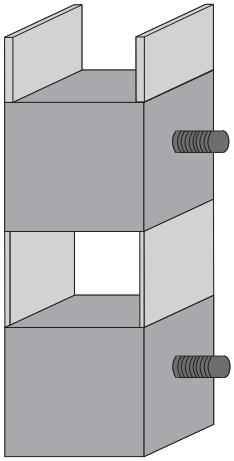

Figure 2.6: The system including impact rods

As can be seen in the figures, doing measurements will not cause big problems using this design because it is very open. Because of the same reason, altering the masses or springs is also relatively easy to do. A remark on this design is that the nonlinear springs can be designed in two settings, first as a clamped-free beam. This construction will lead to a asymmetric 'push' on the masses. The second setting is a clamped-clamped beam construction, in this setting the 'push'will be in the direction of movement of the masses which will improve the response of the system. A downside to this second setting is that the stiffness of the clamped-clamped beam is greater than that of the clamped-free beam. This will probably result in very thin leafsprings.

Finally, the hanging masses design is judged on the earlier determined design criteria:

Design Criterium	Judgement
movement	+
complexity	++
implementation of backlash	++
parameter variation	++
accessibility (for e.g. sensors)	++
compatibility with simulations	++
appearance	+

2.4 Design 3: Rotating masses

The third design uses rotation of the masses instead of translation. The global representation of this design is shown in the figure below.

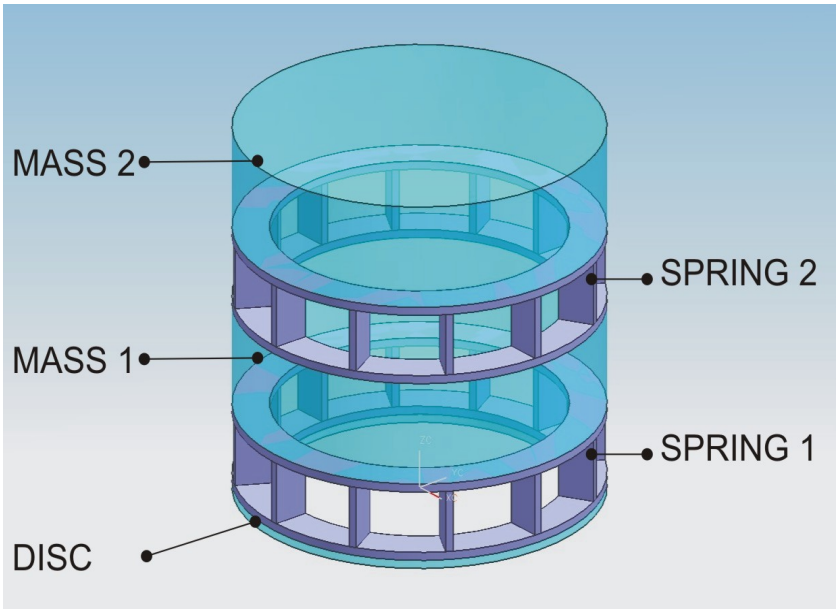

Figure 2.7: Design 3: Rotating masses

In this figure the round discs represent the masses. The springs between the shaker and mass 1 and between both masses consist of thin rings between which vertical leafsprings are attached. In the horizontal plane, all leafsprings are directed towards the center of the masses, as shown in figure 2.7. This configuration will eliminate lateral movement in the x- and y-direction. The only problem is that there will be a small movement in the z-direction due to bending of the leafsprings. An advantage of this design is that backlash can simply be implemented in this system. This can be done by attaching three small blocks of material on the sides of the moving bodies at an angle of 120° with respect to each other (Fig. 2.8).

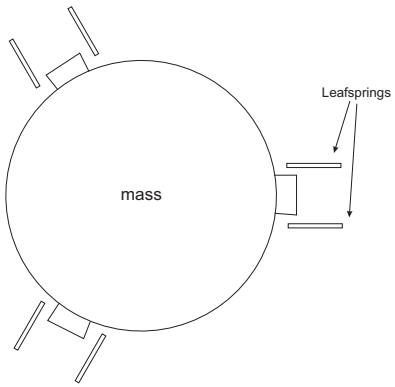

Figure 2.8: Design 3: Rotating masses

Now these blocks can collide with leafsprings that are attached to a stiff construction that is fixed on the shaker. Because there is no external construction to support the masses (which was the case in the previous designs) there is enough space to design a construction around the system.

From a simulation point of view, this type of design is not the most convenient. This is because of the fact that the models made and the simulations that are already done are all tuned to a system with translational movement. So a drawback of this design is that all the numerical analyzes done in the previous chapter cannot be directly applied. A rotational simulation model has to be build and analyzed.

Another disadvantage is that the shaker at hand can not produce a rotational movement directly. Which implies that a new shaker has to be designed or the current shaker has to be adapted in order to use this design.

In conclusion, below the judgements on the design criteria for this third design are listed:

Design Criterium	Judgement
movement	+
complexity	-
implementation of backlash	++
parameter variation	+
accessibility (for e.g. sensors)	++
compatibility with simulations	- -
appearance	+

2.5 Design 4: Linear movement of the masses

With all designs shown above, movement of the masses in an undesired direction (perpendicular to its desired direction) is always possible. Because it is hard to predict how severely this will influence the experiments that have to be done on the prototype, for this last design it is the goal to design a construction in which there is only one degree of freedom per mass.

The main concept behind this design is the double parallelogram of leafsprings from [4]. To achieve a good movement the masses will be symmetrical and all parallelograms will be constructed in threefold at an angle of 120° with respect to each other. The basic concept of this construction is depicted in figure 2.9

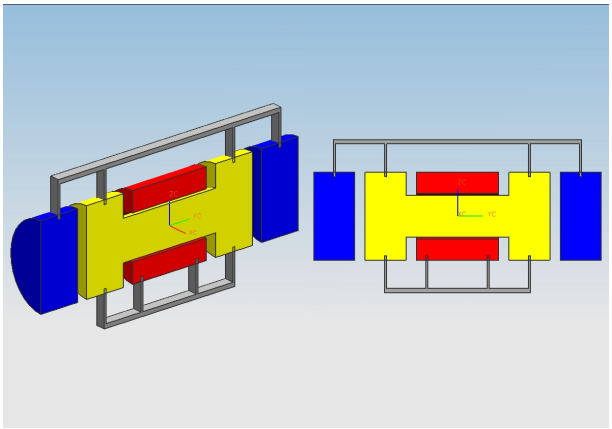

Figure 2.9: linear movement cilinders

In this figure only two parallelograms are shown, between the shaker and mass 1 and between both masses. The configuration of parallelograms around the body of each moving mass is shown in figure 2.10. Using this configuration the masses can only move in the desired direction.

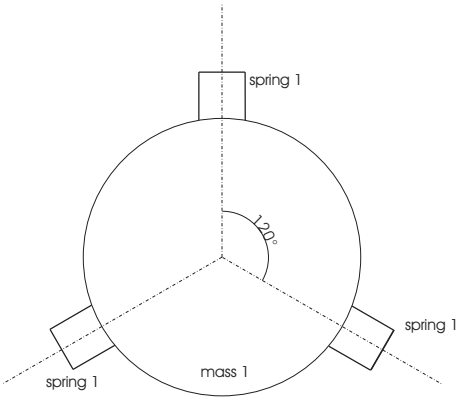

Figure 2.10: Springs under an angle of 120°

To get more insight in this design the concepts explained above are worked out in Unigraphics to create a more detailed and better scaled model. The resulting model in shown in figure 2.16. It clearly shows that when using these concepts, which in theory create a perfect 2 degrees of freedom system, the model becomes very complex.

The advantages and disadvantages of this fourth design are summarized below:

Design Criterium	Judgement
movement	++
complexity	- -
implementation of backlash	- -
parameter variation	- -
accessibility (for e.g. sensors)	- -
compatibility with simulations	++
appearance	+/-

2.6 Elaboration on designs

From the designs described in the previous sections two designs are chosen for a further examination. The designs chosen, are the hanging masses design from section 2.3 and design 4 from section 2.5. These two designs are chosen because the hanging masses design has the best overall performance on the design criteria and the design from 2.5 is the only design that results in a perfect linear movement. First the design with a linear movement of the masses will be examined.

2.6.1 Detailed study of design 4: Linear movement of the masses

In this section a detailed study of an experimental system based on design 4 is explained. In this study the application of the concepts explained above are discussed and applied.

First the geometrical design of the moving masses used, is evaluated. Because the leafsprings need to be attached to the masses, the cylindrical shape is replaced by a hexagonal one. With this form, each set of springs has a flat surface on which they can be mounted.

To avoid that the system will rust stainless steel is used as material. All parts are made of the same material, so that heat variations will not affect the orientation of the parts according to each other. This will improve the measurements.

The masses used in this design are shown in figure 2.11. Mass 2 has a hole at the center, through which the connection rod of mass 1 goes. The hole has a diameter of 15 mm. With the mass set to 1 kg, the length of mass 2 is 87.8 mm. As told, mass 1 has a connection rod with a diameter of 10 mm. To prevent the masses touching each other while oscillating, a backlash of 2.5 mm on each side of the connection rod is introduced. Because of the linear movement of the masses this should be enough. The clearance at both sides of mass 1 (gaps with respect to the base) is 20 mm, which should be enough to implement the backlash and nonlinear springs. The length of the connection rod between the hexagonal masses (mass 1) is 127.8 mm. The length of each weight at the end of the connection rod will be 36 mm. Also visible in the figure below are the additional blocks both masses. These blocks will collide with the nonlinear springs to provide the backlash. Where and how this backlash is applied will be explained further on.

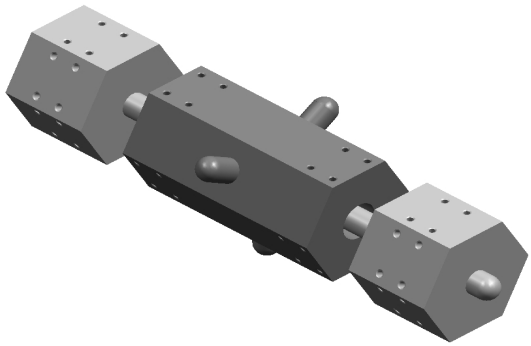

Figure 2.11: Assembly of both masses

The leafsprings and mounting plates are shown in figure 2.12. The mounting plates exactly fit on the flat (width = 25 mm) sides of the hexagonal shaped masses. To mount the springs on the masses, 4 bolts per spring are used. This also implies that threaded holes have to be made in the masses.

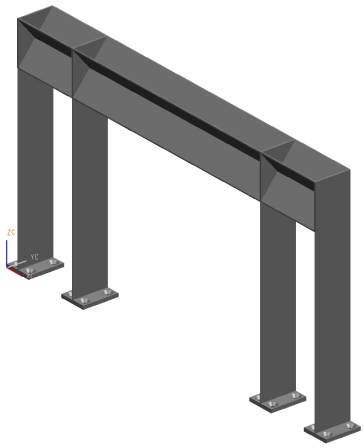

Figure 2.12: Assembly leafsprings

The width of the leafspring is 25 mm and the length is 100 mm. The length has to be of this order because else the linear movement will not be achieved. Each set of springs consist of 12

leafsprings. For the determination of the stiffness of the leafsprings the following equations will be used:

$$c_{xx} = 12\frac{EI}{l^3} \tag{2.1}$$

With:

$$I = \frac{wt^3}{12} \tag{2.2}$$

t is the thickness.
w is the width.
l is the length.

The total stiffness of the spring between the shaker and the first mass has to be approximately 8735 N/m. With $l = 100$ mm, $w = 25$ mm and $n_{spring} = 12$, the thickness t (in mm) of the leafsprings can be calculated:

$$t_1 = \sqrt[3]{\frac{c}{n_{springs}}\frac{l^3}{Ew}} = 0.52\text{mm} \tag{2.3}$$

The total stiffness of the springs between both masses has to be approximately 11150 N/m. With $h = 100$ mm, $b = 25$ mm and $n_{spring} = 12$, the thickness t of the leafsprings can be calculated:

$$t_2 = \sqrt[3]{\frac{c}{n_{springs}}\frac{l^3}{Ew}} = 0.57\text{mm} \tag{2.4}$$

The connection between the leafsprings is constructed of a cross beam as shown in the cross section below. The thickness of the crossbeam components is 1 mm.

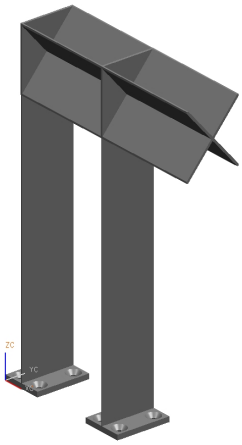

Figure 2.13: Cross-section of the leafspring assembly

This construction is chosen because this will release the leafsprings of inner tension because of misalignment. This will result in a linear movement even if the springs are slightly misaligned.

To attach the construction on the oscillation table at hand a frame is developed on which the masses and springs can be mounted. This body is bolted to the oscillating table as shown in the figure below.

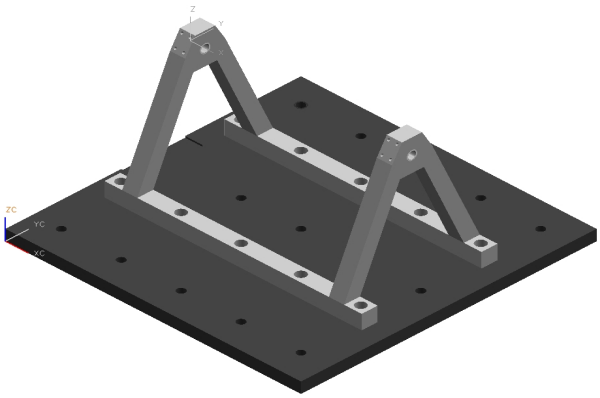

Figure 2.14: Base frame on the oscillation table

The next step is to implement the backlash and nonlinear springs. The backlash on the first mass can be added to the system by attaching springs to the end of the frame. Adding backlash to the second mass is more difficult and for this a new frame has to be designed. The design of this part is done in such a way that it will not interfere with the leafspring assemblies that are mounted on the masses. The result of this is shown in the figure below.

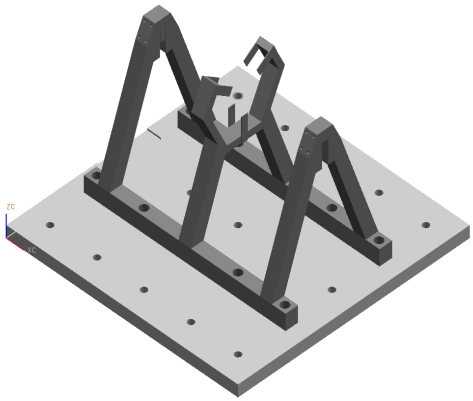

Figure 2.15: Addition of backlash frame for second mass

Now all features of the construction are dimensioned the total assembly can be made. The total assembly is shown below.

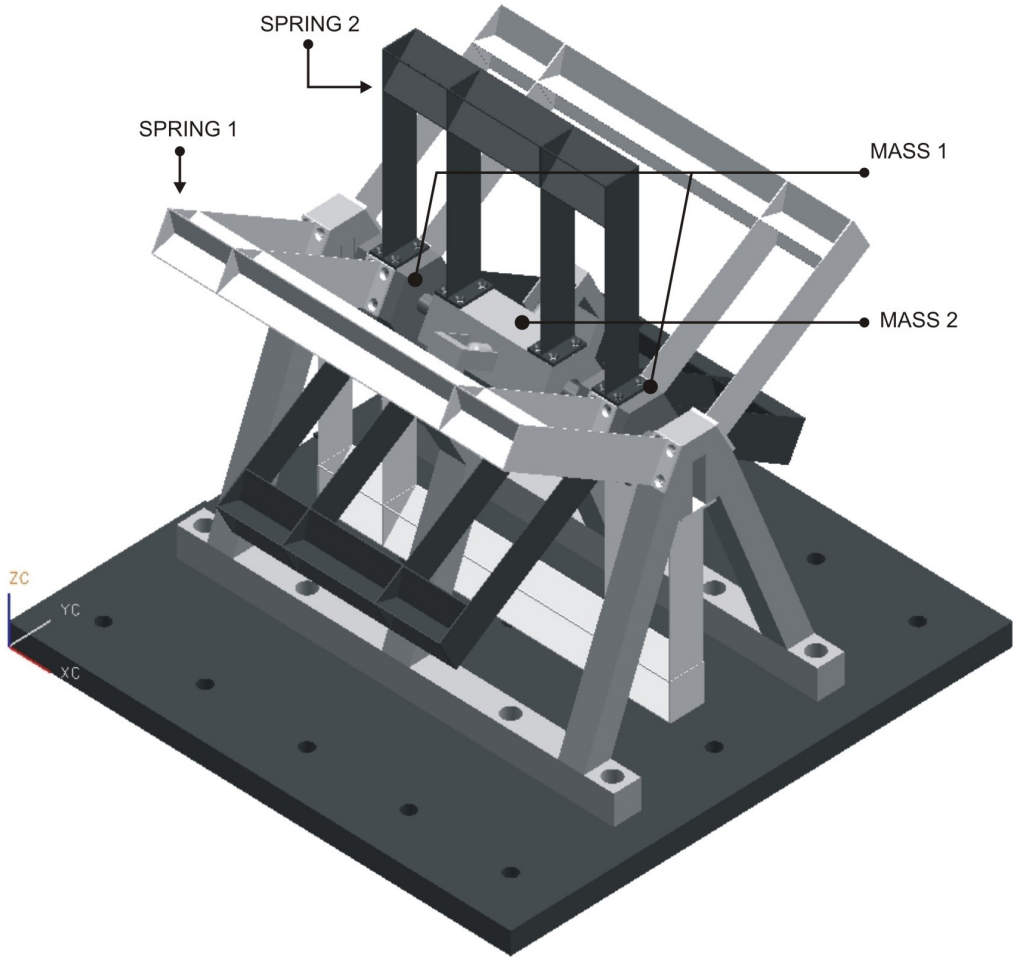

Figure 2.16: Assembly of both masses

Looking at this detailed construction, it is clear that the moving masses are only a small part of the total construction. To check whether this design is useful, the mass of the springs is calculated. This is done to see whether the springs are small enough to be considered as 'massless' springs (as in the model that the design must represent).

First the springs between the base and the first mass are considered. The dimensions of the leaf-springs used are:
$t = 0.52$ mm
$w = 25$ mm
$l = 100$ mm

this gives a mass (per spring) of:

$$m_{s1} = t \cdot w \cdot l \cdot \rho = 1.027e^{-2}\text{kg} \tag{2.5}$$

second the springs between the two mass are considered. The dimensions of the leafsprings used are:
$t = 0.57$ mm
$w = 25$ mm
$l = 100$ mm

this gives a mass (per spring) of:

$$m_{s2} = t \cdot w \cdot l \cdot \rho = 1.126e^{-2}\text{kg} \tag{2.6}$$

For the mass of the each cross member a approximation is made:

$$m_{ci} = 2 \cdot t \cdot \sqrt{2w^2} \cdot l_i \cdot \rho \tag{2.7}$$

For the two leafspring assemblies: $l_{c1} = 255.8$ mm and $1_{c2} = 160.8$ mm. This leads to a mass of:

$$m_{c1} = t \cdot \sqrt{2w^2} \cdot l_{c1} \cdot \rho = 0.0505\text{kg} \tag{2.8}$$

$$m_{c2} = t \cdot \sqrt{2w^2} \cdot l_{c2} \cdot \rho = 0.0318\text{kg} \tag{2.9}$$

For the total mass of the parallel leafspring assembly between the base and mass this gives:

$$m_{leaf1} = 12m_{s1} + 3m_{c1} = 0.275\text{kg} \tag{2.10}$$

And for the total mass of the parallel leafspring assembly between both masses this gives:

$$m_{leaf1} = 12m_{s1} + 3m_{c1} = 0.231\text{kg} \tag{2.11}$$

This evaluation shows that the 'leafspring assemblies' used in this design probably can not be considered as massless springs. Which leads to the conclusion that the total design explained above will probably not resemble the dynamical model used in the simulations. The correctness of this can be evaluated using a different simulation model.

2.6.2 Detailed study of design 2: The hanging masses design

Next, the hanging masses design will be worked out. The advantage is that the design is quite simple, so the dimensioning is a lot easier than in the previous section. First, the size of the masses is calculated. When both masses are fixed at $1kg$, the material is stainless steel and the masses are chosen to be square, the dimensions are:

$$l = w = h = \sqrt[3]{\frac{1}{\rho}} = 0.05[m] \tag{2.12}$$

Next, the dimensions of all leafsprings in the design must be determined. First the sizes of the leafsprings that represent the 'linear' springs k_1 and k_2 are calculated. The springs must have a stiffness of respectively 8735 and 11150 N/m. The material used is stainless steel and the width is fixed at the width of the mass (0.05 m). To get the springs as identical as possible, they must be made out of the same sheet material. For this matter the thickness of the springs is fixed, in this case at t=0.0004 m, so we get:

$$l_1 = \sqrt[3]{\frac{Ehb^3}{k_1}} = 2.64 \cdot 10^{-2}[m] \tag{2.13}$$

$$l_2 = \sqrt[3]{\frac{Ehb^3}{k_2}} = 2.43 \cdot 10^{-2}[m] \tag{2.14}$$

The 'nonlinear' springs k_{1d}, k_{1u}, k_{2d} and k_{2u} are calculated in the same way. With k_{1d}=k_{1u}=$6k_1$=$5.24 \cdot 10^4 N/m$, k_{2d}=k_{2u}=$6k_2$=$6.69 \cdot 10^4 N/m$, the width fixed at $w = 0.01m$ and the length at $l = 0.03m$, we get:

$$t_{1d} = t_{1u} = \sqrt[3]{\frac{6k_1 l^3}{Eh}} = 8.91 \cdot 10^{-4}[m] \tag{2.15}$$

$$t_{2d} = t_{2u} = \sqrt[3]{\frac{6k_2 l^3}{Eh}} = 9.67 \cdot 10^{-4}[m] \tag{2.16}$$

Now all system dimensions are known, the size of the portal can be determined. In figure 2.17 a cross-section of the design is depicted.

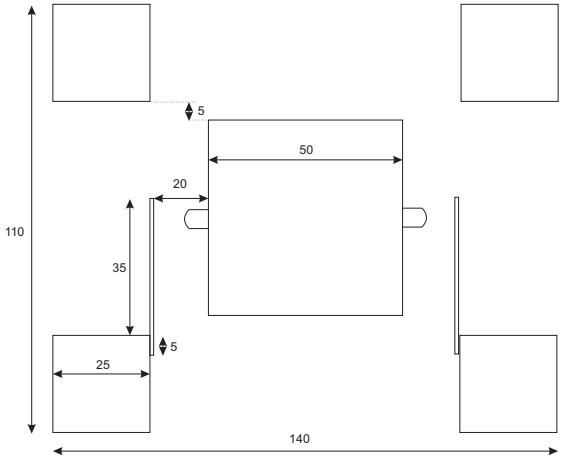

Figure 2.17: Cross-section of the hanging masses design

In the figure all measures of the total design can be found (in mm). The backlash between the masses and the 'nonlinear' springs is 20 mm. With the length of the 'linear' springs as calculated above, it is not possible to implement a large backlash. With a length for the springs of about 25 mm, the mass can only travel about 5 mm in a near linear motion. This is not such a big problem, because simulations have proven that large amounts of backlash eliminate most dynamic behavior. This means that it is most interesting to experiment with a backlash of 0 mm or a very small backlash.

The total length of the 'nonlinear' leafsprings becomes 40 mm, while the impact of the mass occurs at a length 30 mm. When the thickness of the 'roof' is chosen to be 25 mm and the clearance between the lower mass and the ground 10 mm, the outer dimensions of the system come down to 110×140×186mm.

It is clear that for this design, the mass of the springs is a lot smaller in comparison with the design of the previous section. The mass of the springs comes down to the following:

$$m_{k1} = 2 \cdot l \cdot w \cdot t \cdot \rho = 2 \cdot 0.0264 \cdot 0.05 \cdot 0.0004 \cdot 7900 = 8.34 \cdot 10^{-3} kg = 8.34g \tag{2.17}$$

$$m_{k2} = 2 \cdot l \cdot w \cdot t \cdot \rho = 2 \cdot 0.0243 \cdot 0.05 \cdot 0.0004 \cdot 7900 = 7.68 \cdot 10^{-3} kg = 7.68g \tag{2.18}$$

Now the mass of the springs in comparison to the total mass is very small and the springs can be regarded as massless. This means this design resembles the theoretical model better than the previous design. The only problem with this design and the chosen dimension is that the amount of backlash that can be implemented is very small. Though this is quite easy to adjust by making the linear springs longer and less wide. Then, of course the rest of the design must be re-scaled too.

2.7 Measuring plan

The goal of this project is to design an experimental setup of a system with backlash and evaluate the dynamical behavior it comprehends. For the evaluation of the system it needs to be compared with simulations. In order to do this the results of the simulations and experimental measurements need to have the same unit. The simulation results and visualization tools developed in chapter 1 can be used to show the results (responses, and amplitude frequency plot) in displacement (m) or in velocity (m/s). If necessary the results can also be transformed into accelerations (m/s^2) using the ODE-function used. Another advantage of the simulation results is that they can be shown in both absolute values (with respect to the fixed world) and relative (with respect to the oscillation table). This leads to a large range of measuring tools that can be used in the experimental setup.

In order to make a good choice for the sensors used to measure the response of the system, a short impression of available sensors is depicted below:

Measuring unit	Dimension	Type of sensor
displacement	$[m]$	LVDT (appendix E.1)
Velocity	$[m/s]$	PVT (appendix E.2)
Acceleration	$[m/s^2]$	Accelerometer (appendix E.3)

To get the best results from the experimental system, the data acquired from the sensors should be directly comparable with the results of the simulations. A choice has to be made in which unit the results will be measured (and thus simulated), to do this a good assessment has to be made with respect to cost, data acquisition, comparability with respect to simulations and user-friendliness. In order to ease this assessment all sensors are briefly explained in the appendix (see table above).

Choosing a suitable sensor for the the experimental setup is beyond the scope of this report

2.8 Recommendations

Out of the 4 designs from the beginning, two designs are worked out further. This has given insight in the problems that can be encountered when actually building the prototype.

Both designs that are worked out have problems, but the linear movement design has the biggest problem of both because of the mass of the springs. This mass is too large to assume as negligible and this must be regarded as a serious problem.

The design of the hanging masses has the problem of the raising of the masses. This is not a problem when the deviation of the mass is small compared to the length of the 'linear' springs. So one must carefully consider what deviations are desired and what dimensions of the design are necessary for these deviations. When this is all taken into account, the design of hanging masses is the best design.

Chapter 3

Conclusion

The ultimate goal of this investigation was to design an experimental prototype that exhibits interesting nonlinear behavior. The numerical analysis resulted in parameters that were used for the design. Subsequently four designs are brought up, of which two have undergone a detailed study. Nevertheless the design is not completely finished. The problems that have been encountered during the design phase have to be used as feedback (new demands on the design) for an adapted numerical analysis to ultimately make improvements on the design. Subsequently the design has to undergo a more thorough study, including for example a finite element analysis. The flowchart that can be used as a guideline for a further investigation is depicted in figure 3.1.

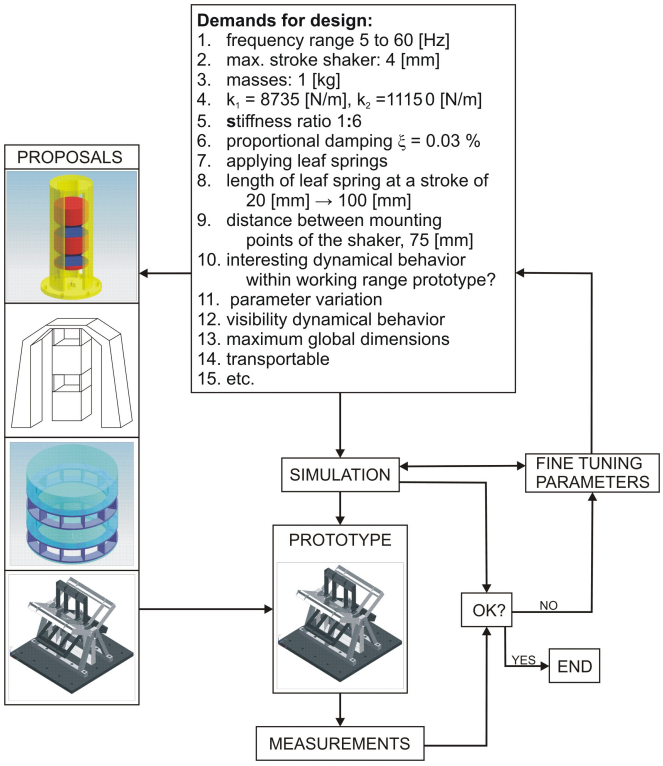

Figure 3.1: Flowchart

Bibliography

[1] E.L.B van de Vorst, D.H. van Campen, A. de Kraker and R.H.B. Fey, *Periodic Solutions of a Multi-DOF beam system with impact*,Journal of Sound and Vibration **192**, 913-925, 1996.

[2] J.M.T. Thompson and H.B. Stewart , *Nonlinear dynamics and chaos*, Chichester, 2002.

[3] P.H.H. Leijendeckers, J.B. Fortuin, F. van Herwijnen and G.A. Schwippert, *Polytechnisch Zakboek*, Doetinchem, 2003.

[4] P.C.J.N. Rosielle and E.A.G. Reker, *Constructieprincipes 1, TUe dictaat nr 0025*, Eindhoven, 2002.

[5] www.kistler.com

[6] www.macrosensors.com

[7] www.wilcoxon.com

[8] www.dimensionengineering.com

Appendix A

MatLab files used for 1DOF system

nonl_1dof.m

The function 'nonl_1dof' contains the equation of motion of the 1DOF system and returns the xdot vector for a given (x,t) vector.

```
function [xdot]=nonl_1dof(t,x)

global x1 x2 k e m b A fbegin fstep fspan

f=(fbegin-fstep+fstep*ceil(t/fspan))*2*pi;

x1=A*sin(f*t) ; x2=A*f*cos(f*t) ;

xdot(1)=x(2);

kd=6*k; ku=6*k; ke=0; s=0;

if (x(1)-x1)<-e ;
    ke=kd ;
    s=-e ;
elseif (x(1)-x1)>e ;
    ke=ku ;
    s=e ;
end

xdot(2)= -(k/m*(x(1)-x1)+ke/m*(x(1)-x1-s)+b/m*(x(2)-x2)) ;

xdot=xdot';
```

ode_rk4.m

The function 'ode_rk4' implements the Runke-Kutta method and uses the function 'nonl_1dof' to calculate the derivative at every time step.

```
function [t,y]=ode_rk4(fun,tspan,h,x0,fname)

global x1 x2 fbegin fstep fspan

%initialize:
y = []; t = []; x = x0 ; I = 0;

% Open file for writing
fid=fopen([fname,'.txt'],'w');

% Run runge-kutta 4th order integration over tspan with fixed-stepsize h
for i=tspan(1):h:tspan(2)

    k1=feval(fun,i,x)';
    k2=feval(fun,i+h/2,x+h.*k1./2)';
    k3=feval(fun,i+h/2,x+h.*k2./2)';
    k4=feval(fun,i+h,x+h.*k3)';
    I=x+h/6*(k1+2*k2+2*k3+k4);
    y=[i,x1,x2,I];
    fprintf(fid,'%e %e %e %e %e \n',y);
    x=I;
end

% close saved data:
fclose(fid); data=load([fname,'.txt']); t=data(:,1);
y=data(:,[2:5]); clear data
```

runme.m

The file 'runme.m' contains parameter values and starting values and runs 'ode_rk4' to solve the ODE for these values.

```
clear all; close all;

global k b m A e fbegin fstep fspan

% system parameters:
k=8882; m=1; b=5.65; A=0.002; e=1e-2;

% Settings for sine stepping -> f=(fbegin-fstep+fstep*ceil(t/fspan))*2*pi;
fbegin=5; fstep=1; fspan=5; feind=60;

% Save data to filename:
fname='tweeveren_s1e-2';

% Check time for calculation time:
tbegin=cputime;

% Settitngs for ode_rk4:
x0 = [0,0] h = 0.001 fun = 'nonl_1dof'
tspan=[0,(feind-fbegin)/fstep*fspan]
```

```
[t,y]=ode_rk4(fun,tspan,h,x0,fname);
%
frp

tijd=cputime-tbegin

% save data and clear all unneaded variables
clear A b fun k m tbegin x0 save([fname,'.mat']) plotme)
```

Appendix B

MatLab files used to simulate behavior of 2-DOF system

```
function [xdot]=threedof(t,x)

global s1 s2 e1 e2 fbegin fstep fspan x1 x2

f=(fbegin-fstep+fstep*ceil(t/fspan))*2*pi;

m1 = 1 ; m2 = 1 ; k1 = 8735 ; k2 = 1.115e4 ; a  = 2.6279 ; b =
2.6628e-004 ; A  = 1.974 ;

x1 = A*sin(f*t) ;
x2 = A*f*cos(f*t);

k1d = 6*k1; k1u = 0 ; k2d = 0 ; k2u = 0 ;

k1e1=0 ; s1=0 ; k2e2=0 ; s2=0 ;

if (x(1)-x1)<-e1 ;
    k1e1=k1d ;
    s1=-e1 ;
end if (x(1)-x1)>e1 ;
    k1e1=k1u ;
    s1=e1 ;
end if (x(3)-x1)<-e2 ;
    k2e2=k2d ;
    s2=-e2 ;
end if (x(3)-x1)>e2 ;
    k2e2=k2u ;
    s2=e2 ;
end

Qn = [ (a*m1+b*(k1+k2))*(x(2)-x2)-b*k2*(x(4)-x2);
-b*k2*(x(2)-x2)+(a*m2+b*k2)*(x(4)-x2) ];

xdot(2) =
-k1/m1*(x(1)-x1)+k2/m1*(x(3)-x(1))-k1e1/m1*(x(1)-x1-s1)-Qn(1)/m1 ;
```

```
xdot(4) = -k2/m2*(x(3)-x(1))-k2e2/m2*(x(3)-x1-s2)-Qn(2)/m2 ;

xdot(1) = x(2) ; xdot(3) = x(4) ;

xdot=xdot';
```

Appendix C

MatLab files used for visualization of simulations

Drawing a amplitude frequency plot

```
% Function [f,amp] = frp(t,y,xn,type)
%
% This function draws a amplitude frequency plot of the
% system that has been simulated using runme.m
%
% Input values:
%
% t,    array with time obtained from runme.m file
% y,    response of system obtained from runme.m file
% xn,   frp from which mass: 1 = mass 1; 2 = mass 2
% type, which results are used to draw plot frp: 0 = x; 1 = xdot
%
% Output:
%
% f,   array with frequency values
% amp, array with max. response values
%
function [f,amp] = frp(t,y,xn,type)

global fbegin fstep fspan tspan h

amp=[]; f=[]; if xn==1
    if type==0
    fprintf('amplitude frequency plot of max(x_1-x_0) is processed')
    ytext='max(x_1-x_0)';
    xtext='Frequency [Hz]';
    elseif type==1
    fprintf('amplitude frequency plot of max(xdot_1-xdot_0) is processed')
    ytext='max(xdot_1-xdot_0)';
    xtext='Frequency [Hz]';
    end
elseif xn==2
    if type==0
    fprintf('amplitude frequency plot of max(x_2-x_0) is processed')
```

```
    ytext='max(x_2-x_0)';
    xtext='Frequency [Hz]';
    elseif type==1
    fprintf('amplitude frequency plot of max(xdot_2-xdot_0) is processed')
    ytext='max(xdot_2-xdot_0)';
    xtext='Frequency [Hz]';
    end
else fprintf('error with input: xn') end if type>1
    fprintf('error with input: type')
end for i=tspan(1)+fspan:fspan:tspan(2);
    F=fbegin-fstep+fstep*ceil(i/fspan);
    T=1/F;
    dT=ceil(4*T/h);
    dt=i/h;
    if type==0
        Fmax=max(y([dt-dT:dt],xn+2)-y([dt-dT:dt],1));
        Fmin=min(y([dt-dT:dt],xn+2)-y([dt-dT:dt],1));
    elseif type==1
        Fmax=max(y([dt-dT:dt],xn+2)-y([dt-dT:dt],2));
        Fmin=min(y([dt-dT:dt],xn+2)-y([dt-dT:dt],2));
    end
    f=[f;F];
    amp=[amp;Fmax,Fmin];
end figure plot(f,amp(:,1)) xlabel(xtext);ylabel(ytext); grid;
title('Amplitude frequency plot') grid on
```

Drawing a phase portrait including Poincaré points

```
% function phase(i,t,y,n)
%
% This function draws a phase diagram and poincare points of the
% system that has been simulated using runme.m
%
% Input values:
%
% i,    base oscilation frequency to evaluate the results at
% t,    array with time obtained from runme.m file
% y,    response of system obtained from runme.m file
% n,    number of oscilation period's to plot
%
% Output:
%
% figure with phase portrait and poincare points

function phase(i,t,y,n)

global h fspan tspan fbegin fstep figure

F=i; T=1/F; dT=ceil(n*T/h);
dt=ceil((F-fbegin+fstep)/fstep*fspan/h); poinc=[]; for j=1:1:n
poinc=[poinc;y(dt-ceil(j*dT/n),:) , t(dt-ceil(j*dT/n))]; end

plot(y([dt-dT:dt],3),y([dt-dT:dt],4)) hold on
```

```
plot(poinc(:,3),poinc(:,4),'*r') grid

xlabel('x_1 [m]') ylabel('xdot_1 [m/s]') title1=['Phase portrait
and poincare points at ',int2str(i),' Hz']; title(title1)
legend('Phase portrait','Poincare points')
```

Drawing the response and frequency content of the system at a desired frequency

```
% function [freq, power, begin, eind]=dft(omega,t,y,n)
%
% This function draws the response and frequency content of the
% system that has been simulated using runme.m at a desired frequency
%
% Input values:
%
% omega,base oscilation frequency from which the response has to be calculated
% t,    array with time obtained from runme.m file
% y,    response of system obtained from runme.m file
% n,    number of oscilation periods to show resonse of
%
% Output:
%
% 2 figures with respectifly frequency content and response of x_1 and x_0
%
% m-files needed:
%
% fdtp.m
% dft_calc.m
function [freq, power, begin, eind]=dft(omega,t,y,n)

global h fspan tspan fbegin fstep

eind=(omega+1-fbegin)*fspan/h; begin=eind-4/h;

x=y([begin:eind],:); tx=t([begin:eind],:); figure subplot(2,1,2)
plot(tx([length(tx)-ceil(n/(omega*h)):length(tx)]),x([length(tx)-ceil(n/(omega*h)):length(tx)],3)
hold on
plot(tx([length(tx)-ceil(n/(omega*h)):length(tx)]),x([length(tx)-ceil(n/(omega*h)):length(tx)],1)
grid on legend('x_1','x_0') xlabel('time [s]') ylabel('response
[m]') title(['Response with base oscillation ',int2str(omega),'
Hz'])

subplot(2,1,1) [freq,power]=dft_calc(x(:,3),omega,h);
title(['Frequency contents of response x_1 with base oscillation
',int2str(omega),' Hz'])
```

```
function [freq, power]=dft(omega,t,y)
```

```
global h fspan tspan fbegin fstep

eind=(omega+1-fbegin)*fspan/h; begin=eind-4/h;

x=y([begin:eind],:); tx=t([begin:eind],:); figure subplot(2,1,2)
plot(tx([length(tx)-ceil(6/(omega*h)):length(tx)]),x([length(tx)-ceil(6/(omega*h)):length(tx)],3)
hold on
plot(tx([length(tx)-ceil(6/(omega*h)):length(tx)]),x([length(tx)-ceil(6/(omega*h)):length(tx)],1)
grid on legend('x_1','x_0') xlabel('time [s]') ylabel('response
[m]') title(['Response with base oscillation ',int2str(omega),'
Hz'])

subplot(2,1,1) [freq,power]=dft(x(:,3),omega,h); title(['Frequency
contents of response x_1 with base oscillation ',int2str(omega),'
Hz'])
```

```
function [f,Pyy]=dft_calc(x,F,h)

df=1/4; np=1/(df*h); if mod(np,2) >= 1
    np=np+2-mod(np,2);
elseif mod(np,2) < 1
    np=np-mod(np,2);
end

y=x([length(x)-np:length(x)]); n=length(y);

Y = fft(y); Pyy = Y.* conj(Y) / n;


f = [0:df:1/(2*h)+1]; plot(f,Pyy(1:length(f)),'bo-')
xlabel('frequency (Hz)')

axis([0 100 .001*max(Pyy(1:length(f))) max(Pyy(1:length(f)))])
grid on
```

Appendix D

Numerical analysis

When using the data processing files, developed for simulating the systems (1-DOF and 2-DOF), one has to keep close attention to some fundamental settings. To keep the settings at the correct values, when using data of previous simulation, all settings used are stored (together with the simulation results) in a .mat file after each simulation.

A very important setting for data processing is the fixed time step (h). This is because h is used in every data processing file and changing h can change the results of some plots. When plotting the Poincaré points this becomes clear. The Poincaré points are calculated at the end of each oscillation period. When using a h value for which:

$$mod\left(\frac{1}{fh}, 1\right) \neq 0$$

the Poincaré points are not calculated at the same point in every oscillation period. Thus, this will result in a drift of the Poincaré point over the phase portrait. An example of this is represented in the figures below. Here the $1/7^{th}$ subharmonic solution of the 2-DOF system is used to illustrate this phenomenon. The parameters for the two figures can be found in the table below.

	h	f	$\frac{1}{fh}$	$mod\left(\frac{1}{fh}, 1\right)$
Fig. D.1	0.001	43	$1/0.043 = 23.25$	0.25
Fig. D.2	$0.1/3f$	43	$3/0.1 = 30$	0

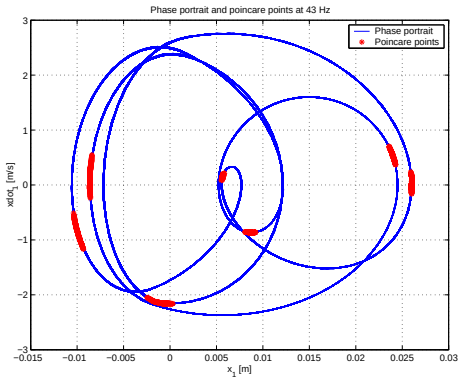

Figure D.1: Phase portrait and Poincaré point at 43 Hz with $h = 0.001$

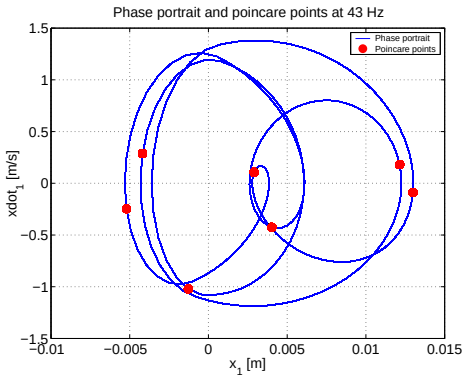

Figure D.2: Phase portrait and Poincaré point at 43 Hz with $h = 0.1/(f * 3)$

When using a badly chosen h value the phase portraits still look good but it is clear that the Poincaré point are drifting away. It is clear that when plotting Poincaré points this has to be kept in mind.

Appendix E

sensors

E.1 LVDT

[6]

The letters LVDT are an acronym for Linear Variable Differential Transformer, a common type of electromechanical transducer that can convert the rectilinear motion of an object to which it is coupled mechanically into a corresponding electrical signal. LVDT linear position sensors are readily available that can measure movements as small as a few millionths of an inch up to several inches, but are also capable of measuring positions up to +/− 0.5 m.

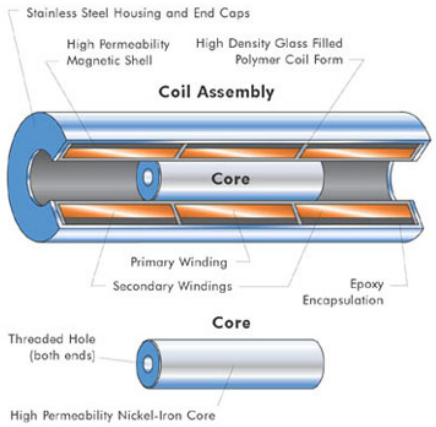

Figure E.1: Basic LVDT components

Figure E.1 shows the components of a typical LVDT. The transformer's internal structure consists of a primary winding centered between a pair of identically wound secondary windings, symmetrically spaced about the primary. The coils are wound on a one-piece hollow form of thermally stable glass reinforced polymer, encapsulated against moisture, wrapped in a high permeability magnetic shield, and then secured in a cylindrical stainless steel housing. This coil assembly is usually the stationary element of the position sensor.

The moving element of an LVDT is a separate tubular armature of magnetically permeable material called the core, which is free to move axially within the coil's hollow bore, and mechanically coupled to the object whose position is being measured. This bore is typically large enough to provide

substantial radial clearance between the core and bore, with no physical contact between it and the coil.

In operation, the LVDT's primary winding is energized by alternating current of appropriate amplitude and frequency, known as the primary excitation. The LVDT's electrical output signal is the differential AC voltage between the two secondary windings, which varies with the axial position of the core within the LVDT coil. Usually this AC output voltage is converted by suitable electronic circuitry to high level DC voltage or current that is more convenient to use.

E.2 PVT

[7]

Velocity Sensors PiezoVelocity Transducers (PVT)

PiezoVelocity Transducers (PVT) are solid state piezoelectric velocity measurement devices. Many vibration analysts prefer to examine vibration signals in terms of velocity (inches per second or ips) to amplify the signal of interest. PVT's inherently decrease high frequency signals allowing better measurement of low frequency vibration. PVT sensors are essentially accelerometers with an internal integration circuit which will produce an output relative to velocity.

System Noise Advantages PVT's can reduce signal noise in many low frequency measurements. The integration circuit amplifies low frequency signals and attenuates high frequency signals. This increases the voltage output at low frequency and filters high frequency noise. The increase in low frequency voltage output reduces the noise contribution of the acquisition equipment. The inherent filtering reduces intermodulation (washover) distortion caused when high frequency signals overload the amplifier and may reduce "ski slope" noise in many applications.

E.3 Accelerometer

[8]

There are many different ways to make an accelerometer! Some accelerometers use the piezoelectric effect - they contain microscopic crystal structures that get stressed by accelerative forces, which causes a voltage to be generated. Another way to do it is by sensing changes in capacitance. If you have two microstructures next to each other, they have a certain capacitance between them. If an accelerative force moves one of the structures, then the capacitance will change. Add some circuitry to convert from capacitance to voltage, and you will get an accelerometer. There are even more methods, including use of the piezoresistive effect, hot air bubbles, and light.

E.3.1 Selection of accelerometer

[5]

Accelerometer Selection Guidelines For Selecting An Accelerometer

To select the accelerometer best suited for an application, a number of variables must be considered to assure that the desired measurement result is obtained. Below is a summary of the more important parameters that should be considered followed by detailed information pertaining to each area.

Frequency Range (Hz): Piezoelectric accelerometers have an upper and lower useable frequency. The upper frequency is determined by the accelerometer's natural frequency and the lower limit by the time constant of the sensor's internal circuitry or external charge amplifier. The accelerometer should be used within the flat portion of the response curve. In this range, the specified sensitivity lies within a defined amplitude tolerance band (usually + 5%).

Measuring Range (+/- 1 g): For low impedance sensors, selection should be such that the expected peak values of acceleration are within the measuring range. If the magnitude of the measuring range is not precisely known, a +/- 500g accelerometer may be used to establish the measurement scale. Then an accelerometer with the applicable range can be selected. Alternatively, it is possible to use a high impedance (charge mode) accelerometer with a charge amplifier to resolve vibration amplitudes over several decades of g levels.

Acceleration Sensitivity (mV/g): The sensitivities listed in catalogs are nominal values. A calibration certificate containing the exact value is provided with each sensor. Since the available full scale voltage is +/- 5 volts, the sensitivity can be determined by dividing the expected acceleration range into the full scale voltage. For example, a +/- 50g range indicates a sensitivity of 100 mV/g.

Operating Temperature Range (°C): High impedance sensors can be used up to 250°C without problems. Due to the limitations of internal electronics, low impedance accelerometers are operable up to 165°C as a maximum.

Ground Isolation: If current loop problems are likely to occur, ground isolated accelerometers are recommended. For example, the ignition of a car engine often causes such problems. This condition can be prevented by selecting a ground isolated unit or installing an adhesive mounting pad under the accelerometer.

Addition of Mass: Adding mass (such as an accelerometer) to a vibrating structure can alter the frequency of the vibration. This is sometimes referred to as "mass loading". As a general rule, the mass of the sensor (and mounting accessories) should not exceed 10% of the mass of the vibrating structure.

Detailed selectinion guidelines The process of selecting an accelerometer for an application encompasses a number of different factors–which are summarized above. Accelerometer designs incorporate a variety of technologies engineered with certain qualities for tailoring the internal parameters towards a specific measurement goal. Kistler accelerometers can be fundamentally classified into three groups which are differentiated by the type of signal conditioning required. These three groups are low impedance piezoelectric, high impedance piezoelectric and variable capacitance.

Technologies: Low Impedance or voltage mode accelerometers contain an internal impedance converter which transforms the high impedance voltage from the sensing element into a usable low impedance voltage signal. These signals are essentially unaffected by triboelectric noise or EMI often generated by cable motion or the environment. High Impedance or charge mode accelerometers are used in conjunction with an external charge amplifier and highly insulated, lownoise cabling is used to isolate the high impedance signals from the environment. Variable Capacitance or K-Beam® accelerometers utilize MEMS technology and the associated integral ASIC conditions the output to a manageable low impedance voltage. Kistler has categorized accelerometers in the product catalog to aid in the selection process. An understanding of important accelerometer characteristics will assure the best choice is made for your specific application. Following, is a list of important parameters for proper accelerometer selection. Reference is made to a particular technology when appropriate.The amplitude measuring range, or expected g level, combined with the frequency.

Appendix F

Material properties

Material properties stainless steel 85% Fe, 0.2% C, 13% Cr (at 293 K):

Density ρ $[kg/m^3]$	$7,8 \times 10^3$
Young 's modulus of elasticity E [Pa]	200×10^9
Coëfficiënt of linear thermal expansion α $[K^{-1}]$	10×10^{-6}
Specific heat c [J/(kg·K)]	460
Coëfficiënt of heat conduction λ $[W/(m \cdot K)]$	27
Melting point [K] ($p = p_0$)	1730
Specific resistance ρ $[\Omega \cdot m]$	720×10^{-9}